Kenya Journal of Sciences

Vol 17 .No.1 2021 Nairobi, Kenya

Series A

Physical and Chemical Sciences

© The Kenya National Academy of Sciences
0250 - 8265 ISSN CODEN KSTSDG

0250 - 8265 ISSN CODEN KSTSDG

Series A Vol.17 No. 1 2021

Kenya Journal of Sciences

Published by the Kenya National Academy of Sciences Founded on November 02, 1983)

Editor-in-Chief
Prof. Bernard O. Aduda

Editors
Prof. R. O. Genga (KJS Series A)
Prof. Kenneth Mavuti (KJS Series B)
Prof. Daniel Rotich (KJS Series C)

Support Staff
Noel L. Abuodha (Mrs)
Edward Ayienda

Layout & Design

Docutech

Kenya Journal of Sciences
A journal of The Kenya National Academy of Sciences published in three series:
Series A (Physical and Chemical Sciences)
Series B (Biological Sciences), and
Series C (Humanities and Social Sciences)

Scope
The journal publishes papers based on original research in both pure and applied sciences and technology, preferably, but not essentially, of relevance to Eastern Africa.

Frequency of Publication
Each series of the journal consists of one volume of two numbers per year.

Correspondence & enquiries
All correspondence concerning manuscripts, reprints, subscription and advertising should be sent to:
The Editor -in- Chief Kenya
Journal of Sciences
P.O. Box 4618 - 00100
Tel: +254-20-311714
Fax: +254-020-311715
Nairobi, Kenya
Email: secretariat@knascience.org
www.knascience.org

Subscription
Members of the Academy receive one. complimentary copy at 30% discount,
Annual subscription rates for each series including surface mail and airmail costs are as follows:

North & South America	**US$ 75**
Australia & New Zealand	**US$ 80**
Europe, Asia & Africa	**US$ 75**
(excluding Kenya)	**US$ 70**
Kenya	**Ksh.500**

Contents

Sensitivity Analysis of Cisco 12000 GSR
Musiga L. A. 1-9

Geometric and Physical Properties of Curvature Tensors
Pokhariyal, G. 10-18

Non-Birth-Death Continuous Time Markov Chain Availability Models withExponentially and Non-Exponentially Distributed Unplanned Outages..
Musiga L. A., Ottieno J. A. M. and Weke P.G. O.....
.....19-35

On Testing the Copernican Principle: Modeling the CMB Temperature Angular Power Spectrum
S. M. Mutunga, G. O. Okeng'o and C. O. Mito
.....36-50

Structure of The Kenya National Academy of Sciences

PARTRON

His Excellency, The President of The Republic of Kenya

THE GOVERNING COUNCIL

1. Prof. Raphael M. Munavu	**Chairman, KNAS**
2. Prof. Ratemo Michieka	**Hon. Secretary, KNAS**
3. Prof. Josephine Ngaira	**Hon. Treasurer, KNAS**
4. Prof. Paul Baki	**Asst. Treasurer**
5. Prof. Kenneth Mavuti	**Asst. Secretary Biological Sciences**
6. Prof. Julius Mwabora	**Asst. Secretary Physical & Chemical Sciences**
7. Prof. Daniel Rotich	**Asst. Humanities & Social Sciences**
8. Prof. Bernard O. Aduda	**Editor - in - Chief**
9. Prof. Waceke Wanjohi	**Asst. Editor - in- Chief**
10. Prof. Mbaabu Mathiu	**Member**
11. Prof. Kenneth Kaduki	**Member**
12. Prof. Joash Aluoch	**Member**
13. CEO NACOSTI	**Ex Officio**
14. Permanent Secretary MOE	**Ex Officio-**
15. Administator KNAS	**Ex Officio**
16. Accountant KNAS	**Ex Officio**

SPECIALISTS COMMITTEES

A. HUMANITIES AND SOCIAL SCIENCES:
Prof. Daniel Rotich Secretary
B. BIOLOGICAL SCIENCES:

Prof. Kenneth Mavuti Secretary
C. PHYSICAL & Chemical SCIENCES:
Prof. Julius Mwabora Secretary

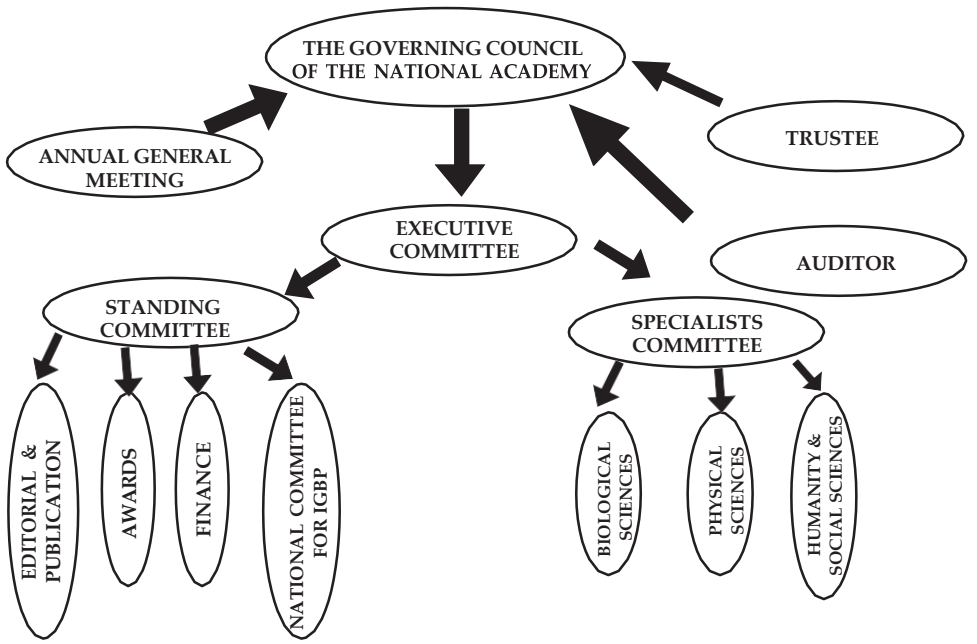

Kenya Journal of Science Series A Vol. 17.no.1 2021

Sensitivity Analysis of Cisco 12000 GSR

Musiga L. A.
School of Mathematics University of Nairobi,
P.O. Box 30197 - 00100
Nairobi Kenya.
Email: lmusiga@uonbi.ac.ke

Abstract
Stochastic models capture the random behavior of the dependability attributes of critical systems. The dependability attributes include availability, reliability, safety, integrity, maintainability, survivability, performance and confidentiality. Stochastic models are used for the estimation of the output measures of interest of critical systems. Generally, changes in the input parameter values result in changes in the model output measures of interest. Parametric sensitivity analysis identifies the input parameter for which the smallest variation implies the greatest impact on the model output measure of interest. Thus parametric sensitivity analysis identifies the system module upon which further research improves the overall system performance. In this paper, the stochastic availability models of Cisco 12000 GSR and the direct method of sensitivity analysis are used to determine the parameter that has the greatest effect on the availability of the system. The results indicate that the repair rate of the clock and scheduler card increases the availability of the system most, hence the Clock Scheduler Card/Switch Fabric Card is the module upon which further research ought to be performed. This would result in the overall improvement of the availability of Cisco 12000 GSR. Mathematica software is used in this work.

Keywords: Sensitivity analysis, direct method, stochastic availability models, output measure, input parameter.

1 Introduction

Stochastic models capture the random behavior of the dependability attributes of critical systems. The dependability attributes include availability, reliability, safety, integrity, maintainability and confidentiality [Avizienis *et al*., 2004]. Additional dependability attributes include survivability and performance [Trivedi et al., 2009]. Stochastic models are useful for the estimation of the output measures of interest of critical systems. Input parameter values are substituted into the stochastic models for the estimation of the relevant output measures of interest. Generally, changes in the input parameter values result in changes in the model output measures of interest. The question of interest to system manufacturers and researchers is whether some of the input parameters, or more specifically, one of the input parameters has the greatest effect on the output measure of interest. The determination of the input parameter which has the greatest effect on the output measure of interest is therefore of paramount importance. Hamby (1994) states that many authors use the terms sensitive, important, most influential, major contributor, effective or correlated when referring to the degree to which an input parameter affects

the model output. Hence, sensitivity analysis techniques identify the most crucial input parameter. The system module to which the identified input parameter belongs is the most critical module of the system. The identified system module is further subjected to research with a view to improving its performance, hence sensitivity analysis serves to guide future research efforts [Hamby, 1994]. The improvement in performance of the system bottleneck results in overall improved system performance. This is the major interest of system manufacturers and researchers. In this paper, the direct method of sensitivity analysis [Hamby, 1994] is applied to the stochastic availability models of Cisco 12000 GSR [Musiga, 2018]. Thus the most critical module of Cisco 12000 GSR, on which further research would result in overall improvement of system performance, is identified. The rest of this paper is organized as follows. Related works on sensitivity analysis are presented in Section 2. In Section 3, the model of the sensitivity analysis technique used in this work is presented. An application to Cisco 12000 GSR is presented in Section 4. The paper concludes with discussions and conclusions in Section 5.

2 Related Work

In this section previous works on sensitivity analysis are presented. In a case study of groundwater decontamination via reductive dechlorination in which the output measure of interest was probability of event occurrence. Stiber *et al.*, (1999) used the Difference in Log-Odds Ratio (ΔLOR) method of sensitivity analysis. Positive ΔLOR implied that the changes in one or more inputs enhanced the probability of the specified event while negative ΔLOR implied that the changes in the inputs caused a reduction in the probability of the event occurring or increased the probability of the event not occurring. The ΔLOR method was used to identify the key input parameter, out of a total of fourteen input parameters, to the groundwater decontamination via reductive dechlorination model. The model input parameters included temperature, pH and whether chemicals such as oxygen, hydrogen, chloride, dichlorethene (DCE) and methane, amongst others were found to be present. The model output measure of interest was the probability that anaerobic degradation of trichloroethene (TCE) via reductive dechlorination occurred. It was found that DCE, which had the largest differences in the log-odds ratio, was the most important determinant of anaerobic degradation of TCE. Another study where sensitivity analysis was performed was the ozone concentration case [Carmichael *et al.*, 1997]. The Automatic Differentiation (AD) technique was used. AD is applicable for large models that involve complex numerical differentiation calculations such as partial derivatives, integral equations and mathematical series. AD was implemented by pre-compilers which analyzed the code of the complex model then automatically added instructions that were needed in order to compute first or higher order derivatives. The expanded code was then compiled so that the code evaluated the function values used in the model, the output measures and the derivatives. Carmichael *et al.*, (1997) used Automatic Differentiation in Fortran (ADIFOR) to calculate the first order sensitivities of ozone concentration with respect to all initial concentrations of eighty-six species and all one hundred and seventy-

eight chemical reaction rate constants, for six different chemical regions. It was found that for the marine region, ozone concentration was most sensitive to the initial concentration of ozone at a normalized sensitivity value of 8.18e-01. With respect to the sensitivity of ozone to variations in the reaction rate constants, the largest sensitivity for the marine region was 0.0671. A sensitivity analysis case study of lamb meat centered on whether the output values varied in a statistically significant manner in association with variation in values for one or more inputs [Carlucci *et al*., 1999]. A model independent probabilistic sensitivity analysis method, namely Analysis of Variance (ANOVA) was used. In the study, a multi-factor ANOVA was used to evaluate the effects of the factors on the response variables. Age at slaughter, storage time and frozen temperature constituted the factors. Ten descriptive terms of odour, flavour and texture were developed in order to determine the sensory profile of lamb meat. Sensory data for each attribute were submitted to an analysis of variance. Each response variable was evaluated using a 0 - 100 scale for different combinations of the inputs. The importance of the input values were evaluated in terms of the relative magnitudes of F values. All of the response variables were significantly affected by the age at slaughter.

In a more recent composite Web service case study, Sato and Trivedi (2007) detected the performance and reliability bottlenecks using the formal sensitivity analysis technique. The composite Web service was a business process called TravelAgent. The business process was implemented in Business Process Execution Language for Web Services (1.1) (BPEL). A Continuous Time Markov Chain (CTMC) model of the composite services, in which failures were incorporated, was developed. A set of Markov models were used to compute the performance (mean response time) and the reliability of Web services and for detecting the system bottlenecks. It was found that upon the failure of the hotel invocation, a restart attempt with the mean overhead time of the mean response time of hotel reservation was sensitive at value 0.247. In a mobile cloud availability case study, three distinct sensitivity analysis techniques were used to detect the bottlenecks of the system [Rubens *et al*., 2015]. The sensitivity analysis techniques used were differential sensitivity analysis, the factorial design of experiments and sensitivity analysis through percentage differences. A hierarchical analytical availability model of the system was developed. Continuous Time Markov Chains were used to model the subsystems. Using differential sensitivity analysis technique, the coverage factor of the spare storage manager was most sensitive at 0.006242686368. Sensitivity analysis based on percentage differences resulted in the number of active storage managers being the most sensitive at 0.0068660546. Battery replacement in the mobile client module was the most sensitive at 0.010521 using the factorial design of experiments technique. A combined analysis for the parameters which appeared among the first five positions in at least two of the three rankings yielded the bottlenecks of the system. The bottlenecks that were extracted from the thirty-six parameters of the hierarchical model were the coverage factors of failures in the active and spare storage managers, the required number of active hosts for the storage managers and the rate of battery replacement after discharge. In the next section, the model of the sensitivity analysis technique used in this work is presented.

3 The Model

Different sensitivity analysis methods are applicable to different types of models [Frey and Patil, 2002]. Sensitivity analysis methods are categorized into three major groups; those that consider one variable at a time, those in which an input matrix is generated yielding an associated output vector and those that partition an input vector depending on the resultant output vector [Hamby, 1994]. Differential sensitivity analysis, also referred to as the direct method, Hamby (1994), is one of the methods of single parameter sensitivity analysis. Sensitivity analysis is easily done when there exists an algebraic equation which relates both the independent and dependent variables. The sensitivity coefficient for an independent variable is computed from the partial derivative of the output measure of interest with respect to the independent variable. Hence the sensitivity coefficient of an output measure Y which is dependent on a parameter is given by

$$S_{\Phi}(Y) = \frac{\delta Y}{\delta \Phi} \tag{1}$$

For a scaled sensitivity analysis the ratio Φ/Y removes the effects of the different units by normalizing the coefficient hence the scaled sensitivity coefficient is given by

$$SS_{\Phi}(Y) = \frac{\Phi}{Y}\frac{\delta Y}{\delta \Phi} \tag{2}$$

In a previous work [Musiga, 2018], the closed-form steady-state availability models of Cisco 12000 GSR were developed. Hence, the direct method of sensitivity analysis is applicable in this work [Hamby, 1994; Hamby, 1995; Loucks and van Beek, 2005]. In the next section, the direct method is applied to the closed form steady-state availability models of Cisco 12000 GSR.

4 An Application

In this section, the direct method of sensitivity analysis and the closed-form steady-state availability models of Cisco 12000 GSR which were developed in [Musiga, 2018] are used to determine the parameter that has the greatest effect on the availability of the system. First, a brief overview of the system description is provided. The Cisco 12000 GSR comprises seven sub-systems or modules, namely, Upgrade, Line Card-in, Line Card-out, Clock and Scheduler Card/Switch Fabric Card, Gigabit Route Processors, Chassis and Cisco IOS modules. The Gigabit Route Processors, IOS and Clock and Scheduler Card/Switch Fabric Card are modules with redundancy. The top level hierarchical model of the system is a block diagram while the lower level models of the modules are Continuous Time Markov Chains. Times to failure and repair are exponentially distributed, coverage factor and switch-over are incorporated in the models where applicable. In subsection 4.1, a summary of the Cisco 12000 GSR steady-state availability models which were developed in [Musiga, 2018] are presented.

4.1 Cisco 12000 GSR Steady-State Availability Models

In this subsection the steady-state availability models which were developed for Cisco 12000 GSR [Musiga, 2018] are presented. The following are the closed-form steady-state availability models for the system and the sub-systems;

(i) System Steady-State Availability Model

$$A_{cisco} = A_{upgrade} x A_{chassis} x A_{LC-in} x A_{LC-out} x A_{GRP} x A_{IOS} x A_{CSC-SFC} \quad (3)$$

where A_{cisco}, $A_{upgrade}$, $A_{chassis}$, $A_{LC\text{-}in}$, $A_{LC\text{-}out}$, A_{GRP}, A_{IOS} and $A_{CSC\text{-}SFC}$ represent the steady-state availabilities of Cisco 12000 GSR system, the Upgrade, Chassis, Line Card-in, Line Card-out, Gigabit Route Processor, IOS Software and Clock and Scheduler Card/Switch Fabric Card Modules, respectively.

(ii) Upgrade Steady-State Availability Model

$$A_{ss}(upgrade) = \frac{1}{1+\frac{\lambda_{upg}}{\mu_{upg}}} \quad (4)$$

where λ_{upg} and μ_{upg} represent the failure and repair rates for the upgrade module, respectively.

(iii) Chassis Steady-State Availability Model

$$A_{ss}(chassis) = \frac{1}{1+\frac{\lambda_{cha}}{\mu_{cha}}} \quad (5)$$

where λ_{cha} and μ_{cha} represent the failure and repair rates for the chassis module, respectively.

(iv) Line Card-In Steady-State Availability Model

$$A_{ss}(LC-in) = \frac{1}{1+\frac{\lambda_{sin}}{\mu_{sin}}+\frac{\lambda_{hin}}{\mu_{hin}}} \quad (6)$$

where λ_{sin} and μ_{sin} represent the failure and repair rates for the software and λ_{hin} and μ_{hin} represent the failure and repair rates for the hardware in the Line Card-In module, respectively.

(v) Line Card-Out Steady-State Availability Model

$$A_{ss}(LC-out) = \frac{1}{1+\frac{\lambda_{sout}}{\mu_{sout}}+\frac{\lambda_{hout}}{\mu_{hout}}} \quad (7)$$

where λ_{sout} and μ_{sout} represent the failure and repair rates for the software and λ_{hout} and μ_{hout} represent the failure and repair rates for the hardware in the Line Card-Out module, respectively.

(vi) Gigabit Route Processor Steady-State Availability Model

$$A_{ss}(GRP) = \frac{1}{E} + \frac{N\lambda_{grp}c_{agrp}}{\beta_{grp}} + \frac{\lambda_{grp}(Nc_{agrp}+c_{sgrp})}{(\mu_{grp}+N\lambda_{grp})E} + \frac{(1-c_{sgrp})}{NE} \quad (8)$$

where

$$E = 1 + \frac{N\lambda_{grp}c_{agrp}}{\beta_{grp}} + \frac{(1-c_{sgrp})}{N} + \frac{\lambda_{grp}(N(1-c_{agrp})+(1-c_{sgrp}))}{\mu_{grp}} + \frac{\lambda_{grp}(Nc_{agrp}+c_{sgrp})}{(\mu_{grp}+N\lambda_{grp})} + \frac{N\lambda_{grp}^2(c_{sgrp}+Nc_{agrp})}{\mu_{grp}(\mu_{grp}+N\lambda_{grp})}$$

and where λ_{grp}, μ_{grp}, c_{agrp}, c_{sgrp}, β_{grp} and N represent the failure rate, repair rate, coverage factor of active units, coverage factor of standby unit, switchover factor and N active units in the Gigabit Route Processor module, respectively.

(vii) IOS Software Steady-State Availability Model

$$A_{ss}(IOS) = \frac{1}{E} + \frac{N\lambda_{ios}c_{aios}}{\beta_{ios}E} + \frac{\lambda_{ios}(Nc_{aios}+c_{sios})}{(\mu_{ios}+N\lambda_{ios})E} + \frac{(1-c_{sios})}{NE} \quad (9)$$

where

$$E = 1 + \frac{N\lambda_{ios}c_{aios}}{\beta_{ios}} + \frac{(1-c_{sios})}{N} + \frac{\lambda_{ios}(N(1-c_{aios})+(1-c_{sios}))}{\mu_{ios}} + \frac{\lambda_{ios}(Nc_{aios}+c_{sios})}{(\mu_{ios}+N\lambda_{ios})} + \frac{N\lambda_{ios}^2(c_{sios}+Nc_{aios})}{\mu_{ios}(\mu_{ios}+N\lambda_{ios})}$$

and where λ_{ios}, μ_{ios}, c_{aios}, c_{sios}, β_{ios} and N represent the failure rate, repair rate, coverage factor of active units, coverage factor of standby unit, switchover factor and N active units in the IOS Software module, respectively.

(viii) Clock Scheduler Card/Switch Fabric Card Steady-State Availability Model

$$A_{ss}(CSC/SFC) = \frac{1}{E} + \frac{2\lambda_1}{\mu_1 E} + \frac{3\lambda_2}{\mu_2 E} \quad (10)$$

where

$$E = 1 + \frac{3\lambda_2}{\mu_2} + \frac{6\lambda_2^2}{\mu_2^2} + \frac{2\lambda_1}{\mu_1} + \frac{2\lambda_1^2}{\mu_1^2} + \frac{6\lambda_1\lambda_2}{\mu_1\mu_2}$$

and where λ_1 and μ_1 represent the failure and repair rates of a Clock Scheduler Card respectively and λ_2 and μ_2 represent the failure and repair rates of a Switch Fabric Card. As is clearly seen from equations (4) - (10), twenty six input parameters are required for the computation of the steady-state availability of Cisco 12000 GSR. The determination of the critical input parameter is the purpose of this paper. In the next subsection, the scaled sensitivity coefficients for the input parameters are computed.

4.2 Sensitivity Analysis

The direct method based on partial derivatives is used to identify the input parameter which has the greatest effect on the system steady-state availability. The partial derivatives of the system steady-state availability with respect to each of the twenty-six input parameters are obtained using Mathematica [Wolfram Mathematica 6]. Input parameter values for Cisco 12000 GSR, which were obtained from [Lee, 2000] and through discussions with Cisco researchers [Trivedi *et al*., 2012], are also fed into Mathematica and scaled sensitivity coefficients are computed. The scaled sensitivity coefficients are ranked in descending order as shown in Table 4.1 overleaf. Discussions and conclusions follow in the subsequent section.

5 Discussions and Conclusions

Sensitivity analysis identifies the bottleneck in a system. The bottleneck is either an activity in or a parameter of the system. The activity or the parameter with the highest sensitivity coefficient is the bottleneck of the system. The identification of the bottleneck assists the system manufacturers and researchers to make improvements either during the design phase or during the operational lifetime of the system. Hence, instigating measures to improve on the bottleneck of a system essentially improves the overall system performance. The system input parameter with the highest scaled sensitivity coefficient should be given the highest priority. Improving the performance of the module to which the identified input parameter belongs improves the whole system performance. From Table 4.1, the input parameter μ_1, which is the repair rate of the Clock and Scheduler Card, has the highest scaled sensitivity coefficient ranking of 0.125001. This implies that a unit increase in the repair rate of the Clock and Scheduler Card leads to a 0.125001 increase in the system steady-state availability. Following closely, the input parameter μ_2 which is the repair rate of the Switch Fabric Card has a scaled sensitivity coefficient ranking of

0.124988. This implies that a unit increase in the repair rate of the Switch Fabric Card leads to a 0.124988 increase in the system steady-state availability. Coincidentally, both input parameters μ_1 and μ_2 belong to the Clock and Scheduler Card/Switch Fabric Card module hence the Clock and Scheduler Card/Switch Fabric Card module is the critical module of Cisco 12000 GSR, it is the bottleneck of the system. Improvements effected on the Clock and Scheduler Card/Switch Fabric Card module would lead to the overall increase in the steady-state availability of the system. In conclusion, the Clock and Scheduler Card/Switch Fabric Card module should be given the highest priority for further research in order to improve the overall system availability of Cisco 12000 GSR.

	Table 4.1 Scaled Sensitivity Coefficients Ranking	
Parameter	**Description**	$\boldsymbol{SS_{\Phi}(Y)}$
μ_1	Repair of Clock Scheduler Card	0.125001
μ_2	Repair of Switch Fabric Card	0.124988
μ_{upg}	Repair of Upgrade	0.000115727
μ_{sin}	Repair of Software Line Card-in	0.0000277765
μ_{sout}	Repair of Software Line Card-out	0.0000277764
c_{aios}	Coverage active unit IOS Software	0.0000277691
c_{sios}	Coverage standby unit IOS Software	0.000027762
μ_{hout}	Repair of Hardware Line Card-out	0.000019341
μ_{hin}	Repair of Hardware Line Card-in	0.0000180091
λ_2	Failure of Switch Fabric Card	0.0000142135
c_{agrp}	Coverage active unit Gigabit Route Processor	0.00000593555
μ_{grp}	Repair of Gigabit Route Processor	0.00000329769
c_{sgrp}	Coverage standby unit Gigabit Route Processor	0.00000254377
μ_{cha}	Repair of Chassis	0.000001261
λ_1	Failure of Clock Scheduler Card	0.00000091694
μ_{ios}	Repair of IOS Software	0.00000000863956
β_{ios}	Switchover in IOS Software	-0.000000000000196954
β_{grp}	Switchover in Gigabit Route Processor	-0.00000000000978687
λ_{ios}	Failure of IOS Software	-0.00000000863936
λ_{cha}	Failure of Chassis	-0.000001261
λ_{grp}	Failure of Gigabit Route Processor	-0.00000329768
λ_{hin}	Failure of Hardware Line Card-in	-0.0000180091
λ_{hout}	Failure of Hardware Line Card-out	-0.000019341
λ_{sout}	Failure of Software Line Card-out	-0.0000277764
λ_{sin}	Failure of Software Line Card-in	-0.0000277765
λ_{upg}	Failure of Upgrade	-0.000115727

References

Avizienis A., J. C. Laprie, B. Randell and C. Landwehr, "Basic Concepts and Taxonomy of Dependable and Secure Computing", *IEEE Trans. Dependable and Secure Computing*, **1**(1), 2004.

Carlucci A., F. Napolitano, A. Girolami, and E. Monteleone, "Methodological approach to evaluate the effects of age at slaughter and storage temperature and time on sensory profile of lamb meat," *Meat Science*, **52**(4):391-395, 1999.

Carmichael G.R., A. Sandu and F.A. Potra, "Sensitivity Analysis for Atmospheric Chemistry Models Via Automatic Differentiation", *Atmospheric Environment*, **31**(3):475-489, 1997.

Frey H. C. and S. R. Patil, "Identification and Review of Sensitivity Analysis Methods", *Risk Analysis*, **22**(3):553-578, 2002.

Hamby D. M.,"A Review of Techniques for Parameter Sensitivity Analysis of Environmental Models", *Environ. Monit. Assess*. 135-154, 1994.

Hamby D. M., "A Comparison of Sensitivity Analysis Techniques", *Health Physics*, **68**(2), 195-204, 1995.

Lee F. Cisco high availability initiatives and related design parameters, 2000.

Loucks D. P. and E. van Beek, "Water Resources Systems Planning and Management: An Introduction to Methods, Models and Applications", 2005.

Musiga L. A., "A Stochastic Hierarchical System Steady-State Availability Model", *Kenya Journal of Sciences*, A, **16**(2) pp. 26-45, 2018.

Rubens M., J. Araujo, D. Oliveira, P. Maciel and K. S. Trivedi, "Sensitivity analysis of a hierarchical model of mobile cloud computing", *Simulation Modelling Practice and Theory*; **50**, 151-164, 2015.

Sato N. and K. S. Trivedi, "Stochastic modeling of composite web services for analysis of their performance and reliability bottlenecks", in ICSOC, 2007.

Stiber N. A., M. Pantazidou and M. J. Small, "Expert System Methodology for Evaluating Reductive Dechlorination at TCE Sites," *Environmental Science and Technology*, **33**(17):3012-3020, 1999.

Trivedi K. S., Kim D. S., Roy A. and D. Medhi, "Dependability and Security Models". Proceedings: DRCN, 2009.

Trivedi K. S., Kim D. S. and R. Ghosh, "System Availability Assessment using Stochastic Models", *Applied Stochastic Models in Business and Industry*, **29**, 94-109, 2012.

Wolfram Mathematica 6. Wolfram research, Inc. http://www.wolfram.com /products/mathematica /index.html.

Kenya Journal of Science Series A Vol. 17.no.1 2021

Geometric and Physical Properties of Curvature Tensors

Pokhariyal, G.P.
School of Mathematics, University of Nairobi,
P.O. Box 30197-00100, Nairobi, Kenya
Email: pokhariyal@uonbi.ac.ke

Abstract
New curvature tensors were introduced by Pokhariyal and Mishra (1971) and Pokhariyal (1982), to study their geometric and relativistic properties. In this paper the relationships of these tensors with other tensors are established. The properties of W_6 tensor and its skew-symmetric as well as symmetric parts are studied in Lorentzian Para Sasakian manifold. The physical properties of W_6 tensor and other tensors are studied in the last section of this paper.

Key words: Curvature tensors, LP-Sasakian manifold, symmetric and skew-symmetric parts.
AMS Subject classification: 53BXX,53CXX

1. Introduction

An *n*- dimensional differentiable manifold *M* is said to be a Lorentzian Para Sasakian (*LP*-Sasakian) manifold, if it admits a *(1,1)* tensor field *F*, a C^∞ vector field *T*, a C^∞ 1-form *A* and a Lorentzian metric g (Matsumoto and Mihai, 1988), which satisfy:

$$A(T) = -1. \tag{1.1}$$

$$\bar{\bar{X}} = X + A(X)T. \tag{1.2}$$

$$g(\bar{X},\bar{Y}) = g(X,Y) + A(X)A(Y). \tag{1.3}$$

$$g(X,T) = A(X),\ \ D_X(T) = \bar{X}. \tag{1.4}$$

$$(D_X F)(Y) = \{g(X,Y) + A(X)A(Y)T\ \ \} + \{X + A(X)T\}A(Y), \tag{1.5}$$

where $\bar{X} \overset{def}{=} F(X).$

In an *LP*-Sasakian manifold *M*, with structure (F,T,A,g), it can be seen (Sasaki,1960) that :

$$\bar{T} = 0, A(\bar{X}) = 0. \tag{1.6}$$

$$rank(F) = n-1. \tag{1.7}$$

Moreover, if we put,

$$F(X,Y) = g(\bar{X},Y), \tag{1.8}$$

then the tensor field $F(X,Y)$ is symmetric in X and Y.

In an *n*-dimensional *LP*-Sasakian manifold, with structure (F,T,A,g), we have (Matsumoto and Mihai, 1988),

$$R(X,Y,Z,T) = g(Y,Z)A(X) - g(X,Z)A(Y), \tag{1.9}$$

$$Ric(X,T) = (n-1)A(X), \tag{1.10}$$

where $R(X,Y,Z,U)$ and $Ric(X,Y)$ denote Riemann curvature tensor and Ricci tensor respectively.

Pokhariyal and Mishra (1971) defined a tensor

$$W_1(X,Y,Z,U) = R(X,Y,Z,U) + \frac{1}{n-1}\big[g(X,U)Ric(Y,Z) - g(Y,U)Ric(X,Z)\big]. \tag{1.11}$$

This tensor W_1 is skew-symmetric in *X* and *Y* and satisfy the cyclic property. Another tensor was defined (Pokhariyal, 1982) as:

$$W_6(X,Y,Z,U) = R(X,Y,Z,U) + \frac{1}{n-1}\big[g(X,Y)Ric(Z,U) - g(X,U)Ric(X,Z)\big]. \tag{1.12}$$

This tensor W_6 does not possess any symmetry, but satisfy the cyclic property. The curvature tensors in the manifold *M* defined as (Yano, 1965):

$$C(X,Y,Z,U) = R(X,Y,Z,U) + \frac{R}{n(n-1)}\big[g(Y,U)g(X,Z) - g(X,U)g(Y,Z)\big], \tag{1.13}$$

$$L(X,Y,Z,U) = R(X,Y,Z,U) \; +$$

$$\frac{1}{n-2}\big[g(X,Z)Ric(Y,U) - g(Y,Z)Ric(X,U) + g(Y,U)Ric(X,Z) - g(X,U)Ric(Y,Z)\big], \tag{1.14}$$

$$V(X,Y,Z,U) = R(X,Y,Z,U) + \frac{1}{n-2}\big[g(Y,U)Ric(X,Z) - g(X,U)Ric(Y,Z)\big]$$

$$+ \frac{R}{(n-1)(n-2)}\big[g(X,U)g(Y,Z) - g(Y,U)g(X,Z)\big], \tag{1.15}$$

and

$$W(X,Y,Z,U) = R(X,Y,Z,U) + \frac{1}{n-1}\big[g(X,Z)Ric(Y,U) - g(X,U)Ric(Y,Z)\big], \quad (1.16)$$

are called concircular, conharmonic, conformal and projective curvature tensors respectively. These tensors satisfy the cyclic properties and corresponding symmetric and skew symmetric properties.

2. Relationship Between Curvature Tensors

In this section, the relationships between the defined tensors have been established. From (1.11), (1.12) and (1.16), we get

$$W(X,Y,Z,U) + W_1(X,Y,Z,U) - W_6(X,Y,Z,U) = R(X,Y,Z,U). \quad (2.1)$$

Using (1.13), (1.14) and (1.15), it was shown (Pokhariyal and Mishra, 1971) that

$$V(X,Y,Z,U) = L(X,Y,Z,U) + \frac{n}{n-2}\big[R(X,Y,Z,U) - C(X,Y,Z,U)\big]. \quad (2.2)$$

Thus, from (2.1) and (2.2), we get

$$W(X,Y,Z,U) + W_1(X,Y,Z,U) - W_6(X,Y,Z,U) - C(X,Y,Z,U) = \frac{n-2}{n}\big[V(X,Y,Z,U) - L(X,Y,Z,U)\big]. \quad (2.3)$$

In the 4-dimensional space M_4 of general relativity (2.3) becomes:

$$W(X,Y,Z,U) + W_1(X,Y,Z,U) - W_6(X,Y,Z,U) - C(X,Y,Z,U) = \frac{1}{2}\big[V(X,Y,Z,U) - L(X,Y,Z,U)\big]. \quad (2.4)$$

3. LP-Sasakian Manifold

In this section, the properties of tensor W_6 and its symmetric and skew-symmetric parts in *LP*-Sasakian manifold are studied. Breaking $W_6(X,Y,Z,U)$ into skew-symmetric and symmetric parts in *X,Y,* we get

$$A(X,Y,Z,U) = \frac{1}{2}\big[W_6(X,Y,Z,U) - W_6(Y,X,Z,U)\big] = R(X,Y,Z,U) + \frac{1}{2(n-1)}\big[g(X,Z)Ric(Y,U) - g(Y,U)Ric(X,Z) - g(Y,Z)Ric(X,U) + g(X,U)Ric(Y,Z)\big] \quad (3.1)$$

and

$$B(X,Y,Z,U)=\frac{1}{2}\left[W_6(X,Y,Z,U)+W_6(Y,X,Z,U)\right]=$$

$$\frac{1}{2(n-1)}\left[g(X,Z)Ric(Y,U)-g(Y,U)Ric(X,Z)+g(Y,Z)Ric(X,U)-g(X,U)Ric(Y,Z)\right]$$

.

(3.2)

Similarly breaking $W_6(X,Y,Z,U)$ into skew-symmetric and symmetric parts in *Z, U*, we get

$$P(X,Y,Z,U)=\frac{1}{2}\left[W_6(X,Y,Z,U)-W_6(X,Y,U,Z)\right]=R(X,Y,Z,U)+$$

$$\frac{1}{2(n-1)}\left[g(X,Z)Ric(Y,U)-g(Y,U)Ric(X,Z)-g(X,U)Ric(Y,Z)+g(Y,Z)Ric(X,U)\right]$$

(3.3)

and

$$Q(X,Y,Z,U)=\frac{1}{2}\left[W_6(X,Y,Z,U)+W_6(X,Y,U,Z)\right]=$$

$$\frac{1}{2(n-1)}\left[g(X,Z)Ric(Y,U)-g(Y,U)Ric(X,Z)+g(X,U)Ric(Y,Z)-g(Y,Z)Ric(X,U)\right],$$

(3.4)

respectively.

Theorem (3.1)

In an *n*-dimensional *LP*-Sasakian manifold, we have

$$W_6(X,Y,Z,T)=g(Y,Z)A(X)-\frac{1}{n-1}A(Y)Ric(X,Z) \tag{3.5a}$$

$$W_6(T,Y,Z,U)=A(U)g(Y,Z)-2A(Z)g(Y,U)+\frac{1}{n-1}A(Z)Ric(Y,U) \tag{3.5b}$$

$$W_6(T,Y,Z,T)=-g(Y,Z)-A(Z)A(Y)=-g(\bar{Y},\bar{Z}). \tag{3.5c}$$

Proof

Putting *U=T* in (1.12) and using (1.4), (1.9) and (1.10), we get (3.5a).
Similarly by putting *X=T* in (1.12) and following the pattern of (3.5a), we get (3.5b).
Putting *X=T* in (3.5a) or *U=T* in (3.5b) and using (1.1) and (1.3), we get (3.5c).

Corollary (3.1)

For a *LP*- Sasakian manifold, we have

$$W_6(\bar{X},\bar{Y},Z,T)=0=W_6(T,Y,\bar{Z},\bar{U}) \quad \text{(b)} \quad W_6(X,Y,T,T)=0=W_6(T,T,Z,U). \tag{3.6a}$$

Proof

Using (1.6) in (3.5a) and (3.5b), we get (3.6a). Using (1.4) and (1.10) in (3.5b) and (3.5b), we get (3.6b).

Theorem (3.2)

In an *n*-dimensional *LP*-Sasakian manifold, we have

$$2A(X,Y,Z,T)=A(X)\left[g(Y,Z)+\frac{1}{n-1}Ric(Y,Z)\right]-A(Y)\left[g(X,Z)+\frac{1}{n-1}Ric(X,Z)\right]$$

(3.7a)

$$2A(T,Y,Z,U)=A(U)\left[g(Y,Z)+\frac{1}{n-1}Ric(Y,Z)\right]$$

$$+A(Z)\left[-3g(Y,U)+\frac{1}{n-1}Ric(Y,U)\right] \tag{3.7b}$$

$$2A(T,Y,Z,T)=-g(Y,Z)-\frac{1}{n-1}Ric(Y,Z)-2A(Y)A(Z). \tag{3.7c}$$

Proof

Putting $U=T$ in (3.1) and using (1.4), (1.9) and (1.10), we get (3.7a).
The proofs of (3.7b) and (3.7c) follows similar pattern.

Corollary (3.2)

On an *LP*-Sasakian manifold, we have

$$A(X,Y,T,T)=0=A(T,T,Z,U) \quad \text{(b)} \quad A(\bar{X},\bar{Y},Z,T)=0=A(T,Y,\bar{Z},\bar{U}). \tag{3.8a}$$

Proof

It follows the pattern of corollary (3.1).

Theorem (3.3)

For a Sasakian manifold, we have

$$2B(X,Y,Z,T)=A(Y)\left[g(X,Z)-\frac{1}{n-1}Ric(X,Z)\right]+A(X)\left[g(Y,Z)-\frac{1}{n-1}Ric(Y,Z)\right] \tag{3.9a}$$

$$2B(T,Y,Z,U)=A(U)\left[g(Y,Z)-\frac{1}{n-1}Ric(Y,Z)\right]-A(Z)\left[g(Y,U)-\frac{1}{n-1}Ric(Y,U)\right]$$

(3.9b)

$$2B(T,Y,Z,T) = \frac{1}{n-1} Ric(Y,Z) - g(Y,Z). \qquad (3.9c)$$

Proof
Putting $U=T$ in (3.2) and using (1.4), (1.9) and (1.10), we get (3.9a). Similarly (3.9b) and (3.9c) can be proved.

Corollary (3.3)
On a *LP*-Sasakian manifold, we have

$$B(X,Y,T,T) = 0 = B(T,T,Z,U) \text{ (b) } B(\bar{X},\bar{Y},Z,T) = 0 = B(T,Y,\bar{Z},\bar{U}).$$

(3.10a)

Proof
Putting $Z=T$ in (3.9a) and $Y=T$ in (3.9b) separately and using (1.4) and (1.10) the (3.10a) is satisfied identically. Using (1.6) in (2.9a) and (3.9b), we get (3.10b).

Theorem (3.4)
In an *n*-dimensional Sasakian manifold, we have

$$2P(X,Y,Z,T) = A(X)\left[3g(Y,Z) - \frac{1}{n-1} Ric(Y,Z)\right]$$

$$- A(Y)\left[g(X,Z) + \frac{1}{n-1} Ric(X,Z)\right]$$

(3.11a)

$$2P(T,Y,Z,U) = A(U)\left[3g(Y,Z) - \frac{1}{n-1} Ric(Y,Z)\right]$$

$$-A(Z)\left[3g(Y,U) - \frac{1}{n-1} Ric(Y,U)\right]$$

(3.11b)

$$2P(T,Y,Z,T) = -3g(Y,Z) + \frac{1}{n-1} Ric(Y,Z) - 2A(Y)A(Z).$$

(3.11c)

Proof
Putting $U=T$ in (3.3) and using (1.4), (1.9) and (1.10), we get (3.11a). The results (3.11b) and (3.11c) can be proved in similar manner.

Corollary (3.4)
On a *LP*- Sasakian manifold, we have

$$P(X,Y,T,T) = 0 = P(T,T,Z,U)$$

(3.12a)

$$P(\bar{X},\bar{Y},Z,T) = 0 = P(T,Y,\bar{Z},\bar{U}).$$

(3.12b)

Proof

Putting $Z = T$ in (3.11a) and using (1.4) and (1.6), we get (3.12a) first part. Similarly putting $Y = T$ and using (1.4) and (1.6) we get the second part of (1.12a). The result (3.12b) can be proved similarly.

Theorem (3.5)

For a *LP*- Sasakian manifold, we have

$$2Q(X,Y,Z,T) = A(Y)\left[g(X,Z) - \frac{1}{n-1}Ric(X,Z)\right] - A(X)\left[g(Y,Z) - \frac{1}{n-1}Ric(Y,Z)\right]$$

(3.13a)

$$(b)2Q(T,Y,Z,U) = A(Z)\left[\frac{1}{n-1}Ric(Y,U) - g(Y,U)\right] + A(U)\left[\frac{1}{n-1}Ric(Y,Z) - g(Y,Z)\right]$$

$$2Q(T,Y,Z,T) = g(Y,Z) - \frac{1}{n-1}Ric(Y,Z).$$

(3.13c)

Proof

Putting *U*=*T* in (3.4) and using (1.4), (1.9) and (1.10), we get (3.13a). The results (3.13b) and (3.13c) can be proved similarly.

Corollary (3.5)

In an *LP*- Sasakian manifold, we have

$$Q(X,Y,T,T) = 0 = Q(T,T,Z,U) \quad \text{(b)} \quad Q(\bar{X},\bar{Y},Z,T) = 0 = Q(T,Y,\bar{Z},\bar{U}).$$

(3.14a)

Proof

The proof follows the pattern of corollary (3.3).

Remark 1

The results for W_6, A, B, P and *Q* symmetric *LP*- Sasakian manifold can be proved as done in (Pokhariyal, 1996). These tensors can also be studied in an *A*-Einstein Sasakian manifold (2001) and other manifolds, like almost decomposable, almost product, almost Kahler and almost Tachibana manifolds (Pokhariyal, 1975). Studying the properties of curvature tensors, in an *n*-dimensional semi-Riemannian manifold (M, g), Tripathi and Gupta (2012) defined τ -curvature tensor as:

$$\tau(X,Y,Z) = a_0R(X,Y)Z + a_1S(Y,Z)X + a_2S(X,Z)Y + a_3S(X,Y)Z + a_4g(Y,Z)QX$$

$$+a_5 g(X,Z)QY + a_6 g(X,Y)QZ + a_7 r\{g(Y,Z)X - g(X,Z)Y\},$$

where $a_0.....a_7$ are real numbers; *R,S,Q* and *r* are the curvature tensor, the Ricci tensor, the Ricci operator and scalar curvature respectively. It was shown that τ - curvature *Pokhariyal, G.P.*

tensor reduces to W_6-curvature tensor if

$$a_0 = 1, a_1 = -a_6 = -\frac{1}{n-1}, a_2 = a_3 = a_4 = a_5 = a_7 = 0.$$

4. Physical Properties

In order to study the physical properties, we define the vector

$$\theta_i = \frac{g_{ij}\varepsilon^{jklm} R_k^p R_{pljm}}{\sqrt{-g} R_{ab} R^{ab}}, \tag{4.1}$$

called the complexion vector of a non-null electromagnetic field with no matter by Misner and Wheeler (1957) and its vanishing implies that field is purely electrical. A semicolon represents covariant differentiation. By setting $W_6{}^h{}_{pml;m} = 0,$ we have from Pokhariyal (1982)

$$R_{pmjl} = R_{pljm}, \tag{4.2}$$

which on substitution in (4.1) implies that $\theta_i = 0.$ Thus, the vanishing of divergence of W_6 in an electromagnetic field reduces to purely electric field.

Rainich (1953) has shown that the necessary and sufficient condition for the existence of the non-null electro-variance are:

$$R = 0, \tag{4.3a}$$

$$R_j^i R_k^j = \frac{1}{4}\delta_k^i R_{ab} R^{ab}, \tag{4.3b}$$

$$\theta_{i,j} = \theta_{j,i}. \tag{4.3c}$$

By replacing R_{ij} by the contacted part W_{6ij} of the tensor W_{6hijk} and other tensors, we can obtain the Rainich conditions.

Remark 2

The Pirani formulation of gravitational waves to the Einstein space can be investigated for W_{6hijk} and all other defined tensors, as done in Pokhariyal (1982).

Discussion

The geometrical and physical properties of the curvature tensor could be attributed to the pattern of the distribution of vector fields over metric potentials and matter tensors. While studying the physical properties, it was shown in a theorem Pokhariyal (1982) that,

"vanishing of the divergence of all those tensors in which the vector field X is present in all the metric potentials, reduces the electromagnetic field to a purely electric field". The tensor W_6 satisfies this property. Further the contracted part of W_6 vanishes in an Einstein space.

References

Matsumoto, K and Mihai, I (1988): On certain transformation in Lorentizian Para Sasiakian manifold; *Tensor, N.S.* 189-197.

Misner, C.W and Wheeler, J.A (1957): *Ann. Phys*. **2**, 525.

Pirani, F.A.E (1962): Recent Developments in General Relativity; Pergamon Press.

Pokhariyal, G.P and Mishra, R.S (1971): Curvature tensors and their relativistic significance II; *Yokhama Math. J.* **19**(2), 97-103.

Pokhariyal, G.P. (1975): Geometric study of a new curvature tensor; *Kyungook Math. Jour*. **15**(1), 67-71.

Pokhariyal, G.P (1982): Relativistic significance of curvature tensors; *International J. Math & Math. Sci*., **5**(1) 133-139.

Pokhariyal, G.P (1996): Curvature tensors in Lorentzian Para Sasakian manifold; *Quaest. Math*., **19**(1-2), 129-136.

Pokhariyal, G.P. (2001): Curvature tensors on A-Einstein Sasakian Manifold; *Balkan Jour. of Geometry*. **6**(1), 45-50.

Rainich, G.Y (1952): *Trans. Am. Maths. Soc*. **27**, 106.

Sasaki, S (1960): On differentiable manifolds with certain structures which are closely related to almost contact structure I; *Tohoku Math. J*. **12**, 456-476.

Tabi, K. (1965): Differential Geometry on Complex and almost complex spaces; Pergamon Press.

Tripathi, M.M and Gupta, P (2012): On $(N(k),\xi)$ Semi-Riemannian Manifold, semi-symmetries; *Int. Elec. Jour. of Geometry*, **5**(1), 42-77.

Kenya Journal of Science Series A Vol. 17.no.1 2021

Non-Birth-Death Continuous Time Markov Chain Availability Models with Exponentially and Non-Exponentially Distributed Unplanned Outages

Musiga L. A., Ottieno J. A. M., and Weke P.G. O.
School of Mathematics, University of Nairobi,
P.O. Box 30197 – 00100, Nairobi, Kenya
Emails: lmusiga@uonbi.ac.ke, joseph.otieno@uonbi.ac.ke, pweke@uonbi.ac.ke

Abstract
Generally mechanical and electronic systems undergo failures and repairs akin to birth-death process. In real life though, systems undergo many failures and repairs which do not transit to the nearest neighbour state, thus are non-birth-death process, the failures of which may either be exponentially or non-exponentially distributed. A lot of research has been conducted on birth-death process. In comparison, little research has been conducted on non-birth-death process thus in this paper a review of research on birth-death process is presented. Since systems undergo many failures and repairs, non-birth-death CTMC availability models for systems with several unplanned outages whose failure distributions are either exponentially or non-exponentially distributed are derived. Specifically non-birth-death CTMC availability models for systems with two exponentially distributed unplanned outages, with three exponentially distributed and three 2-stage hypoexponentially distributed unplanned outages and with four 2-stage hypoexponentially distributed unplanned outages are derived.

Keywords: Non-birth-death process, Continuous Time Markov Chains (CTMC), Availability, Exponential, Hypoexponential, Unplanned outages.

1. Introduction

The advent of the industrial revolution led to the manufacture of mechanical and electronic devices which perform repetitive functions accurately. Unfortunately, the devices suffer from failures occasionally thus necessitating repair services. An engineering system comprises of different modules which have components that undergo failures and repairs, akin to a birth-death process which has been an area of major concern to researchers. In real life though, systems usually undergo many different types of failures and repairs, which are not necessarily to the nearest neighbour, referred to as non-birth-death process [Trivedi, 2001]. Since very little has been done on non-birth-death process, related works on birth-death process are presented in section 2, which are categorized into single birth-death process, pure birth process, pure death process and multiple births process.

The remainder of this paper is organized as follows. Section 2 gives a review previous

works on birth-death process and in section 3 the theory of non-exponentially distributed outages is presented. In section 4 the non-birth-death CTMC availability models with exponentially and non-exponentially distributed unplanned outages is derived. Section 5 forms the discussion of this work and the paper concludes in section 6.
Musiga L. A., Ottieno J. A. M., and Weke P.G. O.

2. Related Works

2.1 Single Birth-Death process

Kendall (1948) obtained solutions for a generalized birth-death process. The differential-difference equation was solved using a partial differential equation for a probability generating function. The expected population size and the solution for which the fluctuation was a minimum was determined.

Karlin and McGregor (1958) defined a linear growth birth-death process. They observed that various aspects of the processes received considerable attention. The generating function formulae in Meixner polynomials and Laguerre systems were used to derive explicit formulae for the transition probabilities. It was found that not all linear growth processes were directly related to the Meixner and Laguerre polynomial systems.

Morgan (1979) presented three alternative approaches for solving CTMC processes with discrete states. The simple linear birth-death process and the immigration process were solved using four alternative approaches, namely; by the Kolmogorov forward equations and directly solving the Lagrange partial differential equation for the probability generating function, by solving the same Lagrange equation using Laplace transforms, via the Kolmogorov backward equations and by using Integral equations.

Novozhilov *et al.* (2005) observed that a fruitful and diverse mathematical field inspired by biology was the theory of birth-death process. Early models in population biology were noted to be largely deterministic. The authors discussed birth-death process as applied to biological problems in evolutionary genomics by considering processes that had one or two absorbing or reflecting states. Further diverse biological processes could be modelled using birth-death process.

A study based on the financial markets by Cont *et al*. (2010) observed that the mechanical nature of execution of orders and the availability of data made order-driven markets interesting candidates for stochastic modelling. Models of order book dynamics were noted to provide insight into the interplay between order flow, liquidity and price dynamics. At the application level, the models provided a quantitative framework in which investors and trading desks could optimize trade execution strategies. Cont *et al*. (2010) focused on the conditional probabilities of events given the state of the order book. They proposed a single birth-death process model for the dynamics of a limit order book. Matrix computations and Laplace transform method were used for computing the probabilities of events. Simulation results illustrated the reliability of the model for the asymptotic behaviour of the limit order book.

Another study in which birth-death process was applied to epidemiological clusters of *Mycobacterium tuberculosis* was conducted by Doss *et al*. (2010). They presented a novel expectation-maximization algorithm for fitting linear birth-death-immigration models with covariates to panel data. The expectation-maximization algorithm was tested on

simulated data followed by focus on the problem of estimating the birth and death rates of the transposable element IS*6110* in *Mycobacterium tuberculosis*. It was found that the East-Asian *Mycobacterium tuberculosis* was evolving at a slower rate than its European-American counterpart. They included *Mycobacterium tuberculosis* drug-resistance status and Human Immunodeficiency Virus infection status of each patient as birth and death rate covariates and found that the lineage remained the only variable that significantly affected IS*6110* birth and death rates.

2.2 Pure Birth Process

A study on fractional pure birth process was conducted by Orsingher and Polito (2010). Fractional equations of various types proved to be useful in representing different phenomena in optics, transport of charge carriers and in economics. They showed that for the linear birth process, the mean values were increasing functions as the order of fractionality decreased. Hence the fractional birth process was useful in the representation of rapidly expanding populations.

Barraza (2016) proposed a Software Reliability model based on a pure birth process. The birth (failure) rate of the process was considered to be non-dependent on time but dependent non-linearly on the previous number of births (failures). The empirical Bayes framework was used to get the birth (failure) rate. In the study, either the mean time to failure was estimated or the stochastic failure process was simulated. The results of a simulation of the model to real gnome open source data from Bugzilla were shown graphically.

2.3 Pure Death Process

Gibson and Renshaw (2001) considered the problem of parameter estimation for immigration-death models when only death times were observed. They derived the parameter likelihood for the immigration-death model given observed removal times only. The analysis was extended to more complex models where immigrants arrived in pairs. This enabled the investigation of parameter likelihoods for the models which had previously been examined using Markov chain Monte Carlo algorithms to accommodate the unobserved processes. The results presented highlighted the difficulty of designing a Markov chain Monte Carlo sampler which could reliably explore the parameter posterior density for the model with paired immigration; a finding which was anticipated would hold for many stochastic compartment models. Gillespie and Renshaw (2005) posed the fascinating question of whether it was possible to determine the fundamental structure of a hidden stochastic process purely from counts of escaping individuals. They developed a general theory of batch immigration counting processes. First, they considered the probability and moment structure of the general linear immigration-death process in

which batches of immigrants arrived randomly. General expressions were then developed for the population size cumulants and probabilities, together with those for the associated counting process. The authors found that high quality inferences on the hidden population process could be inferred purely from externally counted observations.
Musiga L. A., Ottieno J. A. M., and Weke P.G. O.

Gillespie and Renshaw (2008) used immigration regimes to illuminate the intriguing features of an underlying stochastic process. The work first explored paired-immigration and triple-immigration schemes. Detailed analysis of specific cases yielded far more transparent solutions. Further, the authors noted that extending the single- and paired-immigration to *k*-immigration produced intriguing mathematical results which demonstrated that both the approach and the associated conclusions carried over neatly to the multiple-immigration scenario.

2.4 Multiple Births Process

According to Huang and Kercheval (2011), the high-frequency behavior of the limit order book was a natural candidate for stochastic modeling. They noted that the Cont *et al*. (2010) model restricted orders of the order book to unit size. One of the most important conditioning variables for price impact was the size of an order relative to the volume at the best price, so a model that could deal with multiple order sizes was of particular interest. Huang and Kercheval (2011) modelled the limit order book events for multiple order arrivals. Laplace transform was used to develop the stochastic multiple births model.

3. Theory of Non-Exponentially Distributed Outages

Cao *et al*. (2002) began the study of non-exponentially distributed system outages by obtaining the availability model of a system with a single exponentially distributed unplanned outage. All the state transitions, the occurrences of outages and the completions of recoveries from outages, corresponded to Markov renewal moments $\mathbf{T} = \{T_k; k = 0,1,2, \ldots\}$, with the discrete time embedded Markov chain, , $\mathbf{Y} = \{Y_k; k = 0,1,2, \ldots\}$, such that $Y_k$was the system state at time $T_k +$, implying that $Y_k = Z(T_k) +$. The bivariate process $(\mathbf{Y_k}, \mathbf{T_k})$ was a Markov renewal sequence. Hence, $\{Z(t)\}$ was a semi-Markov Process. The non-null elements appeared only in the first row and first column of the Kernel matrix $\mathbf{K(t)}$, corresponding to all possible transitions in a single step. Therefore,

$$K(t) = \begin{pmatrix} 0 & K_{0,1}(t) & \cdots & K_{0,n}(t) \\ K_{1,0}(t) & 0 & \cdots & 0 \\ \vdots & \vdots & \ddots & \vdots \\ K_{n,0}(t) & 0 & \cdots & 0 \end{pmatrix} \tag{1}$$

The non-null elements were derived by induction thus, where TTO represents Time to Outage;

$$K_{0,i}(t) = Pr\{Y_1 = i, T_1 \leq t | Y_0 = 0\}$$

$=$

$Pr\{outage\ i\ is\ the\ first\ one\ to\ occur\ to\ a\ working\ system\ within\ time\ t\}$

$= Pr\{T_1 = TTO_i < TTO_l, l = 1,2, \dots n\ and\ l \neq i\}$

$= \int_0^t Pr\{x < TTO_l, l = 1,2, \dots, n\ and\ l \neq i\} dF_i(x)$

Non-Birth-Death Continuous Time Markov Chain

$= \int_0^t \prod_{l=1, l\neq i}^{n} \big(1 - F_l(x)\big) dF_i(x), i = 1,2, \dots, n$

(2)

And

$K_{i,0}(t) = Pr\{Y_1 = 0, T_1 \leq t \leq | Y_0 = i\}$

$= Pr\{T_1 = TTR_i < t\}$

$= G_i(t), i = 1,2, \dots, n$

(3)

The matrix

$$P = \lim_{t\to\infty} \big[K(t)\big]$$

(4)

was the 1-step transition probability matrix of the embedded Markov chain of the semi-Markov process thus

$$P = \lim_{t\to\infty} \big[K(t)\big]$$

$$= \begin{pmatrix} 0 & P_{0,1}(t) & \cdots & P_{0,n}(t) \\ P_{1,0}(t) & 0 & \cdots & 0 \\ \vdots & \vdots & \ddots & \vdots \\ P_{n,0}(t) & 0 & \cdots & 0 \end{pmatrix}$$

(5)

$$P_{0,i} = K_{0,i}(\infty)$$

$$= \int_0^\infty \prod_{l=1, l\neq i}^{n} \big(1 - F_l(x)\big) dF_i(x), i = 1,2, \dots, n$$

(6)

$$P_{i,0} = K_{i,0}(\infty)$$

$$= G_i(\infty)$$

$$= 1, i = 1, 2, \ldots, n$$
(7)

Since state 0 was the only state in which the system was functional, then the availability, *Musiga L. A., Ottieno J. A. M., and Weke P.G. O.*

A, was given by

$$A = p_0$$
$$= \lim_{t \to \infty} \Pr\{Z(t) = 0 \mid Z(0) = l\} \in \Omega$$
(8)

where Ω was the state space $\{0,1,2, \ldots, n\}$, state 0 being the functional state, and Z(t) was the underlying stochastic process of the system. Hence, where TTO_i, $F_i(x)$, $G_i(t)$ and E_i were the time to outage of type i, cumulative distribution function (CDF) of time to outage of type i and of the time to repair of outage of type i and the mean time to repair (MTTR) of outage of type i,

$$X = min_{i=1,2,\ldots,n}[TTO_i]$$
(9)

Thus

$$F_X(t) = \Pr\{X < t\}$$

$$= \Pr\{\min_{i=1,2,\ldots,n}[TTO_i] < t\}$$
$$= 1 - Pr\{TTO_i > t, \quad for\ i = 1,2, \ldots, n\}$$
$$= 1 - \prod_{l=1}^{n}(1 - F_l(t))$$
(10)

Therefore

$$E_0 = \int_0^\infty \big(1 - F_x(t)\big)dt$$

$$= \int_0^\infty \prod_{l=1}^{n}\big(1 - F_l(t)\big)dt$$
(11)

$$E_i = \int_0^\infty x dG_i(x)dx$$

$$= \int_0^\infty (1 - G_i(x))\, dx, i = 1,2, \ldots, n$$
(12)

Hence the general availability formula was obtained as

$$A = p_0$$

Non-Birth-Death Continuous Time Markov Chain

$$= \frac{E_0}{E_0 + \sum_{i=1}^{n} P_{0,l} E_l}$$

$$= \left[1 + \sum_{i=1}^{n} P_{0,l} \left(\frac{E_l}{E_0} \right) \right]^{-1} \quad (13)$$

The unplanned outage was caused by an unanticipated system failure thus the time to failure (TTF) and the time to repair (TTR) were assumed to be exponentially distributed with parameters MTTF $= \lambda^{-1}$ and MTTR $= \mu^{-1}$, respectively. A planned outage comprised of a system upgrade, maintenance or configuration change that was scheduled to enhance system functionality. The time to planned outage (TTP) and the time to upgrade (TTU) followed general arbitrary distributions with $F_m(t)$ and G(t) as their CDFs, respectively. Figure 3.1 shows the state diagram of the system which was either in state 0 in which the system was working perfectly, state 1 in which the system was under repair following an unplanned failure and state 2 in which the system was undergoing a scheduled upgrade.

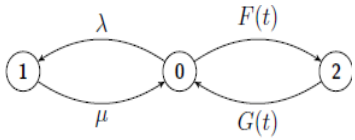

Figure 3.1 State diagram of a system with an unplanned and a planned outage.

Thus, Cao *et al*. (2002) derived the availability model of a system with a single exponentially distributed unplanned outage and a generally distributed planned outage as

$$A = \left(1 + \frac{\lambda}{\mu} + \frac{\lambda}{\mu_2} \cdot \frac{\alpha(\lambda)}{1-\alpha(\lambda)}\right)^{-1} \quad (14)$$

Where $\alpha(\lambda)$ was the Laplace transform of the TTP evaluated at $s = \lambda$.

4. The Models

In the following subsections, the non-birth-death CTMC availability models for systems with two exponentially distributed unplanned outages, with three exponentially distributed and three 2-stage hypoexponentially distributed unplanned outages and with four 2-stage hypoexponentially distributed unplanned outages are derived.

4.1 Continuous Time Markov Chain Availability Model for Two Exponentially Distributed Unplanned Outages

Consider a system with up state 0 and two failed states 1 and 2 with failure and repair rates λ_1, λ_2, μ_1 and μ_2, respectively, as shown in Figure 4.1. Let the TTP be generally distributed with CDF $F_m(t)$ and let the TTU rate be μ_m.

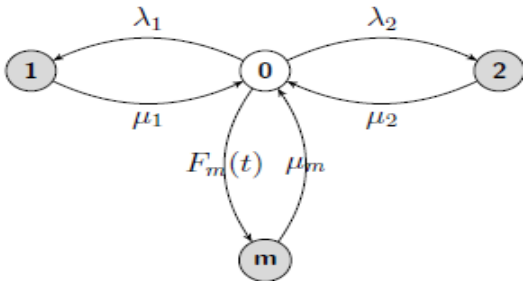

Figure 4.1. State diagram of a system with 2 exponentially distributed unplanned outages and a generally distributed planned outage.

Then the availability model of a system with two exponentially distributed unplanned outages is given by

$$A = \left(1 + \frac{\lambda_1}{\mu_1} + \frac{\lambda_2}{\mu_2} + \frac{\lambda_m}{\mu_m}\right)^{-1} \tag{15}$$

4.2 Continuous Time Markov Chain Availability Model for Three Exponentially Distributed and Three 2-Stage Hypoexponentially Distributed Unplanned Outages

Consider a system with up state 0 and six failed states 1, 2, 3, 4, 5 and 6, with failure and repair rates λ_1, $\lambda_2, \lambda_3, \lambda_4, \lambda_5, \lambda_6, \lambda_7, \lambda_8, \lambda_9, \mu_1, \mu_2, \mu_3, \mu_4, \mu_5$ and μ_6, respectively, where failures into states 1, 2 and 3 are exponentially distributed and failures into states 4, 5 and 6 are 2-stage hypoexponentially distributed, with interim states int_1, int_2 and int_3, as shown in Figure 4.2. Let the TTP be generally distributed with CDF $F_m(t)$ and let the TTU rate be μ_m.

Then the availability model of a system with three exponentially distributed and three 2-stage hypoexponentially distributed unplanned outages is given by

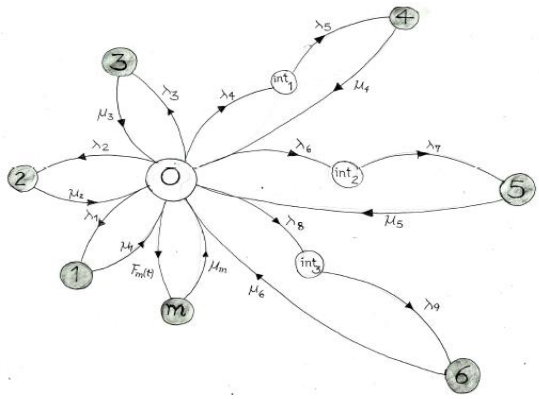

Figure 4.2 State diagram of a system with 3 exponentially and three 2-stage hypoexponentially distributed unplanned outages and a generally distributed planned outage.

$$
\begin{aligned}
A = \Bigg\{ 1 + \frac{1}{(\lambda_5-\lambda_4)(\lambda_7-\lambda_6)(\lambda_9-\lambda_8)} \Bigg\{ \left(\prod_{i=1,2,3} \frac{\lambda_i}{\mu_i} \right) \Bigg\{ \frac{\prod\limits_{i=5,7,9} \lambda_i}{\sum\limits_{i=1,2,3,4,6,8} \lambda_i} \left(1 - \frac{\lambda_m}{\lambda_m + \sum\limits_{i=1,2,3,4,6,8} \lambda_i} \right) \\
- \frac{\prod\limits_{i=5,7,8} \lambda_i}{\sum\limits_{i=1,2,3,4,6,9} \lambda_i} \left(1 - \frac{\lambda_m}{\lambda_m + \sum\limits_{i=1,2,3,4,6,9} \lambda_i} \right) - \frac{\prod\limits_{i=5,6,9} \lambda_i}{\sum\limits_{i=1,2,3,4,7,8} \lambda_i} \left(1 - \frac{\lambda_m}{\lambda_m + \sum\limits_{i=1,2,3,4,7,8} \lambda_i} \right) \\
+ \frac{\prod\limits_{i=5,6,8} \lambda_i}{\sum\limits_{i=1,2,3,4,7,9} \lambda_i} \left(1 - \frac{\lambda_m}{\lambda_m + \sum\limits_{i=1,2,3,4,7,9} \lambda_i} \right) - \frac{\prod\limits_{i=4,7,9} \lambda_i}{\sum\limits_{i=1,2,3,5,6,8} \lambda_i} \left(1 - \frac{\lambda_m}{\lambda_m + \sum\limits_{i=1,2,3,5,6,8} \lambda_i} \right) \\
+ \frac{\prod\limits_{i=4,7,8} \lambda_i}{\sum\limits_{i=1,2,3,5,6,9} \lambda_i} \left(1 - \frac{\lambda_m}{\lambda_m + \sum\limits_{i=1,2,3,5,6,9} \lambda_i} \right) + \frac{\prod\limits_{i=4,6,9} \lambda_i}{\sum\limits_{i=1,2,3,5,7,8} \lambda_i} \left(1 - \frac{\lambda_m}{\lambda_m + \sum\limits_{i=1,2,3,5,7,8} \lambda_i} \right) \\
- \frac{\prod\limits_{i=4,6,8} \lambda_i}{\sum\limits_{i=1,2,3,5,7,9} \lambda_i} \left(1 - \frac{\lambda_m}{\lambda_m + \sum\limits_{i=1,2,3,5,7,9} \lambda_i} \right) \Bigg\}
\end{aligned}
$$

$$+\left\{\frac{\prod\limits_{i=4,5,7,9}\lambda_i}{\sum\limits_{i=1,2,3,4,6,8}\lambda_i}\left(1-\frac{\lambda_m}{\lambda_m+\sum\limits_{i=1,2,3,4,6,8}\lambda_i}\right)-\frac{\prod\limits_{i=4,5,7,9}\lambda_i}{\sum\limits_{i=1,2,3,5,6,8}\lambda_i}\left(1-\frac{\lambda_m}{\lambda_m+\sum\limits_{i=1,2,3,5,6,8}\lambda_i}\right)\right.$$
$$-\frac{\prod\limits_{i=4,5,7,8}\lambda_i}{\sum\limits_{i=1,2,3,4,6,9}\lambda_i}\left(1-\frac{\lambda_m}{\lambda_m+\sum\limits_{i=1,2,3,4,6,9}\lambda_i}\right)+\frac{\prod\limits_{i=4,5,7,8}\lambda_i}{\sum\limits_{i=1,2,3,5,6,9}\lambda_i}\left(1-\frac{\lambda_m}{\lambda_m+\sum\limits_{i=1,2,3,5,6,9}\lambda_i}\right)$$
$$\left.-\frac{\prod\limits_{i=4,5,6,9}\lambda_i}{\sum\limits_{i=1,2,3,4,7,8}\lambda_i}\left(1-\frac{\lambda_m}{\lambda_m+\sum\limits_{i=1,2,3,4,7,8}\lambda_i}\right)+\frac{\prod\limits_{i=4,5,6,9}\lambda_i}{\sum\limits_{i=1,2,3,5,7,8}\lambda_i}\left(1-\frac{\lambda_m}{\lambda_m+\sum\limits_{i=1,2,3,5,7,8}\lambda_i}\right)\right.$$

$$+\frac{\prod_{i=4,5,6,8}\lambda_i}{\sum_{i=1,2,3,4,7,9}\lambda_i}\left(1-\frac{\lambda_m}{\lambda_m+\sum_{i=1,2,3,4,7,9}\lambda_i}\right)-\frac{\prod_{i=4,5,6,8}\lambda_i}{\sum_{i=1,2,3,5,7,9}\lambda_i}\left(1-\frac{\lambda_m}{\lambda_m+\sum_{i=1,2,3,5,7,9}\lambda_i}\right)\Bigg\}\times\left\{\frac{1}{\mu_4}\right\}$$

$$+\left\{\frac{\prod_{i=5,6,7,9}\lambda_i}{\sum_{i=1,2,3,4,6,8}\lambda_i}\left(1-\frac{\lambda_m}{\lambda_m+\sum_{i=1,2,3,4,6,8}\lambda_i}\right)-\frac{\prod_{i=5,6,7,9}\lambda_i}{\sum_{i=1,2,3,4,7,8}\lambda_i}\left(1-\frac{\lambda_m}{\lambda_m+\sum_{i=1,2,3,4,7,8}\lambda_i}\right)\right.$$

$$-\frac{\prod_{i=5,6,7,8}\lambda_i}{\sum_{i=1,2,3,4,6,9}\lambda_i}\left(1-\frac{\lambda_m}{\lambda_m+\sum_{i=1,2,3,4,6,9}\lambda_i}\right)+\frac{\prod_{i=5,6,7,8}\lambda_i}{\sum_{i=1,2,3,4,7,9}\lambda_i}\left(1-\frac{\lambda_m}{\lambda_m+\sum_{i=1,2,3,4,7,9}\lambda_i}\right)$$

$$-\frac{\prod_{i=4,6,7,9}\lambda_i}{\sum_{i=1,2,3,5,6,8}\lambda_i}\left(1-\frac{\lambda_m}{\lambda_m+\sum_{i=1,2,3,5,6,8}\lambda_i}\right)+\frac{\prod_{i=4,6,7,9}\lambda_i}{\sum_{i=1,2,3,5,7,8}\lambda_i}\left(1-\frac{\lambda_m}{\lambda_m+\sum_{i=1,2,3,5,7,8}\lambda_i}\right)$$

$$+\frac{\prod_{i=4,6,7,8}\lambda_i}{\sum_{i=1,2,3,5,6,9}\lambda_i}\left(1-\frac{\lambda_m}{\lambda_m+\sum_{i=1,2,3,5,6,9}\lambda_i}\right)-\frac{\prod_{i=4,6,7,8}\lambda_i}{\sum_{i=1,2,3,5,7,9}\lambda_i}\left(1-\frac{\lambda_m}{\lambda_m+\sum_{i=1,2,3,5,7,9}\lambda_i}\right)\Bigg\}\times\left\{\frac{1}{\mu_5}\right\}$$

$$+\left\{\frac{\prod_{i=5,7,8,9}\lambda_i}{\sum_{i=1,2,3,4,6,8}\lambda_i}\left(1-\frac{\lambda_m}{\lambda_m+\sum_{i=1,2,3,4,6,8}\lambda_i}\right)-\frac{\prod_{i=5,7,8,9}\lambda_i}{\sum_{i=1,2,3,4,6,9}\lambda_i}\left(1-\frac{\lambda_m}{\lambda_m+\sum_{i=1,2,3,4,6,9}\lambda_i}\right)\right.$$

$$-\frac{\prod_{i=5,6,8,9}\lambda_i}{\sum_{i=1,2,3,4,7,8}\lambda_i}\left(1-\frac{\lambda_m}{\lambda_m+\sum_{i=1,2,3,4,7,8}\lambda_i}\right)+\frac{\prod_{i=5,6,8,9}\lambda_i}{\sum_{i=1,2,3,4,7,9}\lambda_i}\left(1-\frac{\lambda_m}{\lambda_m+\sum_{i=1,2,3,4,7,9}\lambda_i}\right)$$

$$-\frac{\prod_{i=4,7,8,9}\lambda_i}{\sum_{i=1,2,3,5,6,8}\lambda_i}\left(1-\frac{\lambda_m}{\lambda_m+\sum_{i=1,2,3,5,6,8}\lambda_i}\right)+\frac{\prod_{i=4,7,8,9}\lambda_i}{\sum_{i=1,2,3,5,6,9}\lambda_i}\left(1-\frac{\lambda_m}{\lambda_m+\sum_{i=1,2,3,5,6,9}\lambda_i}\right)$$

$$+\frac{\prod_{i=4,6,8,9}\lambda_i}{\sum_{i=1,2,3,5,7,8}\lambda_i}\left(1-\frac{\lambda_m}{\lambda_m+\sum_{i=1,2,3,5,7,8}\lambda_i}\right)-\frac{\prod_{i=4,6,8,9}\lambda_i}{\sum_{i=1,2,3,5,7,9}\lambda_i}\left(1-\frac{\lambda_m}{\lambda_m+\sum_{i=1,2,3,5,7,9}\lambda_i}\right)\Bigg\}\times\left\{\frac{1}{\mu_6}\right\}$$
$$+\Bigg\{\left(\frac{\lambda_m\prod_{i=5,7,9}\lambda_i}{\lambda_m+\sum_{i=1,2,3,4,6,8}\lambda_i}\right)-\left(\frac{\lambda_m\prod_{i=5,7,8}\lambda_i}{\lambda_m+\sum_{i=1,2,3,4,6,9}\lambda_i}\right)-\left(\frac{\lambda_m\prod_{i=5,6,9}\lambda_i}{\lambda_m+\sum_{i=1,2,3,4,7,8}\lambda_i}\right)$$
$$+\left(\frac{\lambda_m\prod_{i=5,6,8}\lambda_i}{\lambda_m+\sum_{i=1,2,3,4,7,9}\lambda_i}\right)-\left(\frac{\lambda_m\prod_{i=4,7,9}\lambda_i}{\lambda_m+\sum_{i=1,2,3,5,6,8}\lambda_i}\right)+\left(\frac{\lambda_m\prod_{i=4,7,8}\lambda_i}{\lambda_m+\sum_{i=1,2,3,5,6,9}\lambda_i}\right)$$
$$+\left(\frac{\lambda_m\prod_{i=4,6,9}\lambda_i}{\lambda_m+\sum_{i=1,2,3,5,7,8}\lambda_i}\right)-\left(\frac{\lambda_m\prod_{i=4,6,8}\lambda_i}{\lambda_m+\sum_{i=1,2,3,5,7,9}\lambda_i}\right)\Bigg\}\left\{\frac{1}{\mu_m}\right\}\Bigg\}$$
$$\div\Bigg\{\frac{\prod_{i=5,7,9}\lambda_i}{\sum_{i=1,2,3,4,6,8}\lambda_i}\left(1-\frac{\lambda_m}{\lambda_m+\sum_{i=1,2,3,4,6,8}\lambda_i}\right)-\frac{\prod_{i=5,7,8}\lambda_i}{\sum_{i=1,2,3,4,6,9}\lambda_i}\left(1-\frac{\lambda_m}{\lambda_m+\sum_{i=1,2,3,4,6,9}\lambda_i}\right)$$
$$-\frac{\prod_{i=5,6,9}\lambda_i}{\sum_{i=1,2,3,4,7,8}\lambda_i}\left(1-\frac{\lambda_m}{\lambda_m+\sum_{i=1,2,3,4,7,8}\lambda_i}\right)+\frac{\prod_{i=5,6,8}\lambda_i}{\sum_{i=1,2,3,4,7,9}\lambda_i}\left(1-\frac{\lambda_m}{\lambda_m+\sum_{i=1,2,3,4,7,9}\lambda_i}\right)$$
$$-\frac{\prod_{i=4,7,9}\lambda_i}{\sum_{i=1,2,3,5,6,8}\lambda_i}\left(1-\frac{\lambda_m}{\lambda_m+\sum_{i=1,2,3,5,6,8}\lambda_i}\right)+\frac{\prod_{i=4,7,8}\lambda_i}{\sum_{i=1,2,3,5,6,9}\lambda_i}\left(1-\frac{\lambda_m}{\lambda_m+\sum_{i=1,2,3,5,6,9}\lambda_i}\right)$$
$$+\frac{\prod_{i=4,6,9}\lambda_i}{\sum_{i=1,2,3,5,7,8}\lambda_i}\left(1-\frac{\lambda_m}{\lambda_m+\sum_{i=1,2,3,5,7,8}\lambda_i}\right)-\frac{\prod_{i=4,6,8}\lambda_i}{\sum_{i=1,2,3,5,7,9}\lambda_i}\left(1-\frac{\lambda_m}{\lambda_m+\sum_{i=1,2,3,5,7,9}\lambda_i}\right)\Bigg\}\Bigg\}^{-1} \quad (16)$$

4.3 Continuous Time Markov Chain Availability Model for Four 2-Stage Hypoexponentially Distributed Unplanned Outages

Consider a system with four failed states 1, 2, 3 and 4, with failure and repair rates $\lambda_1, \lambda_2, \lambda_3, \lambda_4, \lambda_5, \lambda_6, \lambda_7\lambda_8, \mu_1, \mu_2, \mu_3, \mu_4, \mu_5, \mu_6, \mu_7$ andμ_8, in two stages as shown in Figure 4.3. The interim states are int_1, int_2, int_3 and int_4. Let the TTP be generally distributed with CDF $F_m(t)$ and let the TTU rate be μ_m.

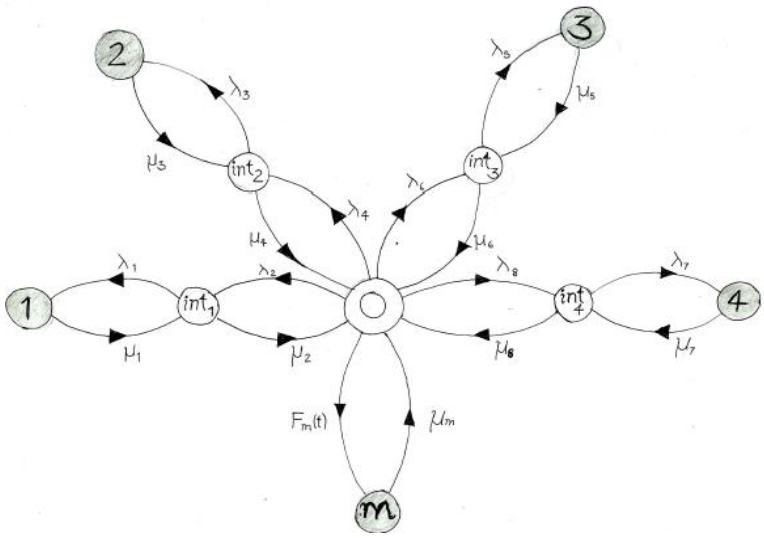

Figure 4.3 State diagram of a system with four 2-stage hypoexponentially distributed unplanned outages and a generally distributed planned outage.

The availability model of a system with four 2-stage hypoexponentially distributed unplanned outages is given by

$$
\begin{aligned}
A = \Bigg\{ 1 + \frac{1}{(\lambda_2-\lambda_1)(\lambda_4-\lambda_3)(\lambda_6-\lambda_5)(\lambda_8-\lambda_7)} \Bigg\{ & \frac{\prod_{i=1,2,4,6,8}\lambda_i}{\sum_{i=1,3,5,7}\lambda_i}\left(1-\frac{\lambda_m}{\lambda_m+\sum_{i=1,3,5,7}\lambda_i}\right) \\
& - \frac{\prod_{i=1,2,4,6,8}\lambda_i}{\sum_{i=2,3,5,7}\lambda_i}\left(1-\frac{\lambda_m}{\lambda_m+\sum_{i=2,3,5,7}\lambda_i}\right) - \frac{\prod_{i=1,2,4,6,7}\lambda_i}{\sum_{i=1,3,5,8}\lambda_i}\left(1-\frac{\lambda_m}{\lambda_m+\sum_{i=1,3,5,8}\lambda_i}\right) \\
& + \frac{\prod_{i=1,2,4,6,7}\lambda_i}{\sum_{i=2,3,5,8}\lambda_i}\left(1-\frac{\lambda_m}{\lambda_m+\sum_{i=2,3,5,8}\lambda_i}\right) - \frac{\prod_{i=1,2,4,5,8}\lambda_i}{\sum_{i=1,3,6,7}\lambda_i}\left(1-\frac{\lambda_m}{\lambda_m+\sum_{i=1,3,6,7}\lambda_i}\right) \\
& + \frac{\prod_{i=1,2,4,5,8}\lambda_i}{\sum_{i=2,3,6,7}\lambda_i}\left(1-\frac{\lambda_m}{\lambda_m+\sum_{i=2,3,6,7}\lambda_i}\right) + \frac{\prod_{i=1,2,4,5,7}\lambda_i}{\sum_{i=1,3,6,8}\lambda_i}\left(1-\frac{\lambda_m}{\lambda_m+\sum_{i=1,3,6,8}\lambda_i}\right) \\
& - \frac{\prod_{i=1,2,4,5,7}\lambda_i}{\sum_{i=2,3,6,8}\lambda_i}\left(1-\frac{\lambda_m}{\lambda_m+\sum_{i=2,3,6,8}\lambda_i}\right) - \frac{\prod_{i=1,2,3,6,8}\lambda_i}{\sum_{i=1,4,5,7}\lambda_i}\left(1-\frac{\lambda_m}{\lambda_m+\sum_{i=1,4,5,7}\lambda_i}\right)
\end{aligned}
$$

$$
\begin{aligned}
&- \frac{\prod_{i=1,2,3,6,8} \lambda_i}{\sum_{i=2,4,5,7} \lambda_i} \left(1 - \frac{\lambda_m}{\lambda_m + \sum_{i=2,4,5,7} \lambda_i}\right) - \frac{\prod_{i=1,2,3,6,7} \lambda_i}{\sum_{i=1,4,5,8} \lambda_i} \left(1 - \frac{\lambda_m}{\lambda_m + \sum_{i=1,4,5,8} \lambda_i}\right) \\
&+ \frac{\prod_{i=1,2,3,6,7} \lambda_i}{\sum_{i=2,4,5,8} \lambda_i} \left(1 - \frac{\lambda_m}{\lambda_m + \sum_{i=2,4,5,8} \lambda_i}\right) - \frac{\prod_{i=1,2,3,5,8} \lambda_i}{\sum_{i=1,4,6,7} \lambda_i} \left(1 - \frac{\lambda_m}{\lambda_m + \sum_{i=1,4,6,7} \lambda_i}\right) \\
&+ \frac{\prod_{i=1,2,3,5,8} \lambda_i}{\sum_{i=2,4,6,7} \lambda_i} \left(1 - \frac{\lambda_m}{\lambda_m + \sum_{i=2,4,6,7} \lambda_i}\right) + \frac{\prod_{i=1,2,3,5,7} \lambda_i}{\sum_{i=1,4,6,8} \lambda_i} \left(1 - \frac{\lambda_m}{\lambda_m + \sum_{i=1,4,6,8} \lambda_i}\right) \\
&- \frac{\prod_{i=1,2,3,5,7} \lambda_i}{\sum_{i=2,4,6,8} \lambda_i} \left(1 - \frac{\lambda_m}{\lambda_m + \sum_{i=2,4,6,8} \lambda_i}\right) \Bigg\} \times \left\{\frac{\mu_1 + \mu_2}{\mu_1 \mu_2}\right\} \\
&+ \frac{\prod_{i=2,3,4,6,8} \lambda_i}{\sum_{i=1,3,5,7} \lambda_i} \left(1 - \frac{\lambda_m}{\lambda_m + \sum_{i=1,3,5,7} \lambda_i}\right) - \frac{\prod_{i=1,2,3,4,6,8} \lambda_i}{\sum_{i=1,4,5,7} \lambda_i} \left(1 - \frac{\lambda_m}{\lambda_m + \sum_{i=1,4,5,7} \lambda_i}\right) \\
&- \frac{\prod_{i=2,3,4,6,7} \lambda_i}{\sum_{i=1,3,5,8} \lambda_i} \left(1 - \frac{\lambda_m}{\lambda_m + \sum_{i=1,3,5,8} \lambda_i}\right) + \frac{\prod_{i=2,3,4,6,7} \lambda_i}{\sum_{i=1,4,5,8} \lambda_i} \left(1 - \frac{\lambda_m}{\lambda_m + \sum_{i=1,4,5,8} \lambda_i}\right) \\
&- \frac{\prod_{i=2,3,4,5,8} \lambda_i}{\sum_{i=1,3,6,7} \lambda_i} \left(1 - \frac{\lambda_m}{\lambda_m + \sum_{i=1,3,6,7} \lambda_i}\right) + \frac{\prod_{i=2,3,4,5,8} \lambda_i}{\sum_{i=1,4,6,7} \lambda_i} \left(1 - \frac{\lambda_m}{\lambda_m + \sum_{i=1,4,6,7} \lambda_i}\right) \\
&+ \frac{\prod_{i=2,3,4,5,7} \lambda_i}{\sum_{i=1,3,6,8} \lambda_i} \left(1 - \frac{\lambda_m}{\lambda_m + \sum_{i=1,3,6,8} \lambda_i}\right) - \frac{\prod_{i=2,3,4,5,7} \lambda_i}{\sum_{i=1,4,6,8} \lambda_i} \left(1 - \frac{\lambda_m}{\lambda_m + \sum_{i=1,4,6,8} \lambda_i}\right) \\
&- \frac{\prod_{i=1,3,4,6,8} \lambda_i}{\sum_{i=2,3,5,7} \lambda_i} \left(1 - \frac{\lambda_m}{\lambda_m + \sum_{i=2,3,5,7} \lambda_i}\right) + \frac{\prod_{i=1,3,4,6,8} \lambda_i}{\sum_{i=2,4,5,7} \lambda_i} \left(1 - \frac{\lambda_m}{\lambda_m + \sum_{i=2,4,5,7} \lambda_i}\right) \\
&+ \frac{\prod_{i=1,3,4,6,7} \lambda_i}{\sum_{i=2,3,5,8} \lambda_i} \left(1 - \frac{\lambda_m}{\lambda_m + \sum_{i=2,3,5,8} \lambda_i}\right) - \frac{\prod_{i=1,3,4,6,7} \lambda_i}{\sum_{i=2,4,5,8} \lambda_i} \left(1 - \frac{\lambda_m}{\lambda_m + \sum_{i=2,4,5,8} \lambda_i}\right) \\
&+ \frac{\prod_{i=1,3,4,5,8} \lambda_i}{\sum_{i=2,3,6,7} \lambda_i} \left(1 - \frac{\lambda_m}{\lambda_m + \sum_{i=2,3,6,7} \lambda_i}\right) - \frac{\prod_{i=1,3,4,5,8} \lambda_i}{\sum_{i=2,4,6,7} \lambda_i} \left(1 - \frac{\lambda_m}{\lambda_m + \sum_{i=2,4,6,7} \lambda_i}\right) \\
&- \frac{\prod_{i=1,3,4,5,7} \lambda_i}{\sum_{i=2,3,6,8} \lambda_i} \left(1 - \frac{\lambda_m}{\lambda_m + \sum_{i=2,3,6,8} \lambda_i}\right) + \frac{\prod_{i=1,3,4,5,7} \lambda_i}{\sum_{i=2,4,6,8} \lambda_i} \left(1 - \frac{\lambda_m}{\lambda_m + \sum_{i=2,4,6,8} \lambda_i}\right) \Bigg\} \times \left\{\frac{\mu_3 + \mu_4}{\mu_3 \mu_4}\right\}
\end{aligned}
$$

$$+\frac{\prod_{i=2,4,5,6,8}\lambda_i}{\sum_{i=1,3,5,7}\lambda_i}\left(1-\frac{\lambda_m}{\lambda_m+\sum_{i=1,3,5,7}\lambda_i}\right)-\frac{\prod_{i=2,4,5,6,8}\lambda_i}{\sum_{i=1,3,6,7}\lambda_i}\left(1-\frac{\lambda_m}{\lambda_m+\sum_{i=1,3,6,7}\lambda_i}\right)$$
$$-\frac{\prod_{i=2,4,5,6,7}\lambda_i}{\sum_{i=1,3,5,8}\lambda_i}\left(1-\frac{\lambda_m}{\lambda_m+\sum_{i=1,3,5,8}\lambda_i}\right)+\frac{\prod_{i=2,4,5,6,7}\lambda_i}{\sum_{i=1,3,6,8}\lambda_i}\left(1-\frac{\lambda_m}{\lambda_m+\sum_{i=1,3,6,8}\lambda_i}\right)$$
$$-\frac{\prod_{i=2,3,5,6,8}\lambda_i}{\sum_{i=1,4,5,7}\lambda_i}\left(1-\frac{\lambda_m}{\lambda_m+\sum_{i=1,4,5,7}\lambda_i}\right)+\frac{\prod_{i=2,3,5,6,8}\lambda_i}{\sum_{i=1,4,6,7}\lambda_i}\left(1-\frac{\lambda_m}{\lambda_m+\sum_{i=1,4,6,7}\lambda_i}\right)$$
$$+\frac{\prod_{i=2,3,5,6,7}\lambda_i}{\sum_{i=1,4,5,8}\lambda_i}\left(1-\frac{\lambda_m}{\lambda_m+\sum_{i=1,4,5,8}\lambda_i}\right)-\frac{\prod_{i=2,3,5,6,7}\lambda_i}{\sum_{i=1,4,6,8}\lambda_i}\left(1-\frac{\lambda_m}{\lambda_m+\sum_{i=1,4,6,8}\lambda_i}\right)$$
$$-\frac{\prod_{i=1,4,5,6,8}\lambda_i}{\sum_{i=2,3,5,7}\lambda_i}\left(1-\frac{\lambda_m}{\lambda_m+\sum_{i=2,3,5,7}\lambda_i}\right)+\frac{\prod_{i=1,4,5,6,8}\lambda_i}{\sum_{i=2,3,6,7}\lambda_i}\left(1-\frac{\lambda_m}{\lambda_m+\sum_{i=2,3,6,7}\lambda_i}\right)$$
$$+\frac{\prod_{i=1,4,5,6,7}\lambda_i}{\sum_{i=2,3,5,8}\lambda_i}\left(1-\frac{\lambda_m}{\lambda_m+\sum_{i=2,3,5,8}\lambda_i}\right)-\frac{\prod_{i=1,4,5,6,7}\lambda_i}{\sum_{i=2,3,6,8}\lambda_i}\left(1-\frac{\lambda_m}{\lambda_m+\sum_{i=2,3,6,8}\lambda_i}\right)$$
$$+\frac{\prod_{i=1,3,5,6,7}\lambda_i}{\sum_{i=2,4,5,7}\lambda_i}\left(1-\frac{\lambda_m}{\lambda_m+\sum_{i=2,4,5,7}\lambda_i}\right)-\frac{\prod_{i=1,3,5,6,7}\lambda_i}{\sum_{i=2,4,6,7}\lambda_i}\left(1-\frac{\lambda_m}{\lambda_m+\sum_{i=2,4,6,7}\lambda_i}\right)$$
$$-\frac{\prod_{i=1,3,5,6,7}\lambda_i}{\sum_{i=2,4,5,8}\lambda_i}\left(1-\frac{\lambda_m}{\lambda_m+\sum_{i=2,4,5,8}\lambda_i}\right)+\frac{\prod_{i=1,3,5,6,7}\lambda_i}{\sum_{i=2,4,6,8}\lambda_i}\left(1-\frac{\lambda_m}{\lambda_m+\sum_{i=2,4,6,8}\lambda_i}\right)\Bigg\}\times\left\{\frac{\mu_5+\mu_6}{\mu_5\mu_6}\right\}$$
$$+\frac{\prod_{i=2,4,6,7,8}\lambda_i}{\sum_{i=1,3,5,7}\lambda_i}\left(1-\frac{\lambda_m}{\lambda_m+\sum_{i=1,3,5,7}\lambda_i}\right)-\frac{\prod_{i=2,4,6,7,8}\lambda_i}{\sum_{i=1,3,5,8}\lambda_i}\left(1-\frac{\lambda_m}{\lambda_m+\sum_{i=1,3,5,8}\lambda_i}\right)$$
$$-\frac{\prod_{i=2,4,5,7,8}\lambda_i}{\sum_{i=1,3,6,7}\lambda_i}\left(1-\frac{\lambda_m}{\lambda_m+\sum_{i=1,3,6,7}\lambda_i}\right)+\frac{\prod_{i=2,4,5,7,8}\lambda_i}{\sum_{i=1,3,6,8}\lambda_i}\left(1-\frac{\lambda_m}{\lambda_m+\sum_{i=1,3,6,8}\lambda_i}\right)$$
$$-\frac{\prod_{i=2,3,6,7,8}\lambda_i}{\sum_{i=1,4,5,7}\lambda_i}\left(1-\frac{\lambda_m}{\lambda_m+\sum_{i=1,4,5,7}\lambda_i}\right)+\frac{\prod_{i=2,3,6,7,8}\lambda_i}{\sum_{i=1,4,5,8}\lambda_i}\left(1-\frac{\lambda_m}{\lambda_m+\sum_{i=1,4,5,8}\lambda_i}\right)$$

$$+\frac{\prod_{i=2,3,5,7,8}\lambda_i}{\sum_{i=1,4,6,7}\lambda_i}\left(1-\frac{\lambda_m}{\lambda_m+\sum_{i=1,4,6,7}\lambda_i}\right)-\frac{\prod_{i=2,3,5,7,8}\lambda_i}{\sum_{i=1,4,6,8}\lambda_i}\left(1-\frac{\lambda_m}{\lambda_m+\sum_{i=1,4,6,8}\lambda_i}\right)$$
$$-\frac{\prod_{i=1,4,6,7,8}\lambda_i}{\sum_{i=2,3,5,7}\lambda_i}\left(1-\frac{\lambda_m}{\lambda_m+\sum_{i=2,3,5,7}\lambda_i}\right)+\frac{\prod_{i=1,4,6,7,8}\lambda_i}{\sum_{i=2,3,5,8}\lambda_i}\left(1-\frac{\lambda_m}{\lambda_m+\sum_{i=2,3,5,8}\lambda_i}\right)$$
$$+\frac{\prod_{i=1,4,5,7,8}\lambda_i}{\sum_{i=2,3,6,7}\lambda_i}\left(1-\frac{\lambda_m}{\lambda_m+\sum_{i=2,3,6,7}\lambda_i}\right)-\frac{\prod_{i=1,4,5,7,8}\lambda_i}{\sum_{i=2,3,6,8}\lambda_i}\left(1-\frac{\lambda_m}{\lambda_m+\sum_{i=2,3,6,8}\lambda_i}\right)$$
$$+\frac{\prod_{i=1,3,6,7,8}\lambda_i}{\sum_{i=2,4,5,7}\lambda_i}\left(1-\frac{\lambda_m}{\lambda_m+\sum_{i=2,4,5,7}\lambda_i}\right)-\frac{\prod_{i=1,3,6,7,8}\lambda_i}{\sum_{i=2,4,5,8}\lambda_i}\left(1-\frac{\lambda_m}{\lambda_m+\sum_{i=2,4,5,8}\lambda_i}\right)$$
$$-\frac{\prod_{i=1,3,5,7,8}\lambda_i}{\sum_{i=2,4,6,7}\lambda_i}\left(1-\frac{\lambda_m}{\lambda_m+\sum_{i=2,4,6,7}\lambda_i}\right)+\frac{\prod_{i=1,3,5,7,8}\lambda_i}{\sum_{i=2,4,6,8}\lambda_i}\left(1-\frac{\lambda_m}{\lambda_m+\sum_{i=2,4,6,8}\lambda_i}\right)\Bigg\}\times\left\{\frac{\mu_7+\mu_8}{\mu_7\mu_8}\right\}$$
$$+\left\{\left(\frac{\lambda_m\prod_{i=2,4,6,8}\lambda_i}{\lambda_m+\sum_{i=1,3,5,7}\lambda_i}\right)-\left(\frac{\lambda_m\prod_{i=2,4,6,7}\lambda_i}{\lambda_m+\sum_{i=1,3,5,8}\lambda_i}\right)-\left(\frac{\lambda_m\prod_{i=2,4,5,8}\lambda_i}{\lambda_m+\sum_{i=1,3,6,7}\lambda_i}\right)+\left(\frac{\lambda_m\prod_{i=2,4,5,7}\lambda_i}{\lambda_m+\sum_{i=1,3,6,8}\lambda_i}\right)\right.$$
$$-\left(\frac{\lambda_m\prod_{i=2,3,6,8}\lambda_i}{\lambda_m+\sum_{i=1,4,5,7}\lambda_i}\right)+\left(\frac{\lambda_m\prod_{i=2,3,6,7}\lambda_i}{\lambda_m+\sum_{i=1,4,5,8}\lambda_i}\right)+\left(\frac{\lambda_m\prod_{i=2,3,5,8}\lambda_i}{\lambda_m+\sum_{i=1,4,6,7}\lambda_i}\right)-\left(\frac{\lambda_m\prod_{i=2,3,5,7}\lambda_i}{\lambda_m+\sum_{i=1,4,6,8}\lambda_i}\right)$$
$$-\left(\frac{\lambda_m\prod_{i=1,4,6,8}\lambda_i}{\lambda_m+\sum_{i=2,3,5,7}\lambda_i}\right)+\left(\frac{\lambda_m\prod_{i=1,4,6,7}\lambda_i}{\lambda_m+\sum_{i=2,3,5,8}\lambda_i}\right)+\left(\frac{\lambda_m\prod_{i=1,4,5,8}\lambda_i}{\lambda_m+\sum_{i=2,3,6,7}\lambda_i}\right)-\left(\frac{\lambda_m\prod_{i=1,4,5,7}\lambda_i}{\lambda_m+\sum_{i=2,3,6,8}\lambda_i}\right)$$
$$\left.+\left(\frac{\lambda_m\prod_{i=1,3,6,8}\lambda_i}{\lambda_m+\sum_{i=2,4,5,7}\lambda_i}\right)-\left(\frac{\lambda_m\prod_{i=1,3,6,7}\lambda_i}{\lambda_m+\sum_{i=2,4,5,8}\lambda_i}\right)-\left(\frac{\lambda_m\prod_{i=1,3,5,8}\lambda_i}{\lambda_m+\sum_{i=2,4,6,7}\lambda_i}\right)+\left(\frac{\lambda_m\prod_{i=1,3,5,7}\lambda_i}{\lambda_m+\sum_{i=2,4,6,8}\lambda_i}\right)\right\}\left\{\frac{1}{\mu_m}\right\}\Bigg\}$$
$$\div\left\{\frac{\prod_{i=2,4,6,8}\lambda_i}{\sum_{i=1,3,5,7}\lambda_i}\left(1-\frac{\lambda_m}{\lambda_m+\sum_{i=1,3,5,7}\lambda_i}\right)-\frac{\prod_{i=2,4,6,7}\lambda_i}{\sum_{i=1,3,5,8}\lambda_i}\left(1-\frac{\lambda_m}{\lambda_m+\sum_{i=1,3,5,8}\lambda_i}\right)\right.$$
$$\left.-\frac{\prod_{i=2,4,5,8}\lambda_i}{\sum_{i=1,3,6,7}\lambda_i}\left(1-\frac{\lambda_m}{\lambda_m+\sum_{i=1,3,6,7}\lambda_i}\right)+\frac{\prod_{i=2,4,5,7}\lambda_i}{\sum_{i=1,3,6,8}\lambda_i}\left(1-\frac{\lambda_m}{\lambda_m+\sum_{i=1,3,6,8}\lambda_i}\right)\right.$$

$$
\begin{aligned}
&-\frac{\prod_{i=2,3,6,8}\lambda_i}{\sum_{i=1,4,5,7}\lambda_i}\left(1-\frac{\lambda_m}{\lambda_m+\sum_{i=1,4,5,7}\lambda_i}\right)+\frac{\prod_{i=2,3,6,7}\lambda_i}{\sum_{i=1,4,5,8}\lambda_i}\left(1-\frac{\lambda_m}{\lambda_m+\sum_{i=1,4,5,8}\lambda_i}\right)\\
&+\frac{\prod_{i=2,3,5,8}\lambda_i}{\sum_{i=1,4,6,7}\lambda_i}\left(1-\frac{\lambda_m}{\lambda_m+\sum_{i=1,4,6,7}\lambda_i}\right)-\frac{\prod_{i=2,3,5,7}\lambda_i}{\sum_{i=1,4,6,8}\lambda_i}\left(1-\frac{\lambda_m}{\lambda_m+\sum_{i=1,4,6,8}\lambda_i}\right)\\
&-\frac{\prod_{i=1,4,6,8}\lambda_i}{\sum_{i=2,3,5,7}\lambda_i}\left(1-\frac{\lambda_m}{\lambda_m+\sum_{i=2,3,5,7}\lambda_i}\right)+\frac{\prod_{i=1,4,6,7}\lambda_i}{\sum_{i=2,3,5,8}\lambda_i}\left(1-\frac{\lambda_m}{\lambda_m+\sum_{i=2,3,5,8}\lambda_i}\right)\\
&+\frac{\prod_{i=1,4,5,8}\lambda_i}{\sum_{i=2,3,6,7}\lambda_i}\left(1-\frac{\lambda_m}{\lambda_m+\sum_{i=2,3,6,7}\lambda_i}\right)-\frac{\prod_{i=1,4,5,7}\lambda_i}{\sum_{i=2,3,6,8}\lambda_i}\left(1-\frac{\lambda_m}{\lambda_m+\sum_{i=2,3,6,8}\lambda_i}\right)\\
&+\frac{\prod_{i=1,3,6,8}\lambda_i}{\sum_{i=2,4,5,7}\lambda_i}\left(1-\frac{\lambda_m}{\lambda_m+\sum_{i=2,4,5,7}\lambda_i}\right)-\frac{\prod_{i=1,3,6,7}\lambda_i}{\sum_{i=2,4,5,8}\lambda_i}\left(1-\frac{\lambda_m}{\lambda_m+\sum_{i=2,4,5,8}\lambda_i}\right)\\
&-\frac{\prod_{i=1,3,5,8}\lambda_i}{\sum_{i=2,4,6,7}\lambda_i}\left(1-\frac{\lambda_m}{\lambda_m+\sum_{i=2,4,6,7}\lambda_i}\right)+\frac{\prod_{i=1,3,5,7}\lambda_i}{\sum_{i=2,4,6,8}\lambda_i}\left(1-\frac{\lambda_m}{\lambda_m+\sum_{i=2,4,6,8}\lambda_i}\right)\Bigg\}\Bigg\}^{-1} \qquad (17)
\end{aligned}
$$

5. Discussion

A system with two exponentially distributed unplanned outages is a system whereby there are two different types of failures, each of which is exponentially distributed. Thus equation 13 is appropriate for the computation of the availability of such a system. In a system where there are three exponentially distributed and three 2-stage hypoexponentially distributed unplanned outages, the failures are of two different types. In the first case, there are three different failures each of which is exponentially distributed and in the second case, there are three other different failures but each of them is hypoexponentially distributed. Regarding hypoexponentially distributed failures, the system first enters a semi-failed state, that is an interim state, where only minimal essential services are provided and due to further degradation, the system finally enters the completely failed state, hence equation 14. For a four 2-stage hypoexponentially distributed unplanned outages there are four different failed states but entry into the failed state is preceded by a semi-failed state. Thus equation 15 is appropriate for computing the availability of such a system.

6. Conclusion

The CTMC availability models for systems with variously distributed unplanned outages; namely two exponentially distributed unplanned outages, three exponentially distributed and three 2-stage hypoexponentially distributed unplanned outages and four 2-stage hypoexponentially distributed unplanned outages have been derived. These models are applicable to systems whose failure distributions follow the distributions considered in

this work. In a subsequent work, the non-birth-death CTMC availability models with exponentially and non-exponentially distributed unplanned outages are applied to an engineering system.

References

Barraza N. R., A New Homogeneous Pure Birth Process based Software Reliability Model, *Software Engineering Companion (ICSE-C)*, IEEE/ACM International Conference, 2016.

Cao Y., Sun H., Trivedi K. S. and Han J. J., System Availability With Non-Exponentially Distributed Outages, *IEEE Transactions on Reliability*, **51**(2), 193-198, 2002.

Cont R., Stoikov S. and Talreja R., A Stochastic Model for Order Book Dynamics, *Operations Research*, **58**, 549 - 563, 2010.

Doss C. R., Suchard M. A., Holmes I., Kato-Maeda M. and Minin V. N., Fitting Birth-Death Processes to Panel Data with Applications to Bacterial DNA Fingerprinting, *The Annals of Applied Statistics*, **7**(4), 2315 - 2335, 2013.

Gibson G. J. and Renshaw E., Inference for Immigration-Death Processes with Single and Paired Immigrants, *Inverse Problems*, **17**, 455-466, 2001.

Gillespie C. S. and Renshaw E., The Evolution of a Batch-Immigration Death Process Subject to Counts, *Proceedings of the Royal Society*, A, **461**, 1563-1581, 2005.

Huang H. and Kercheval A. N., A Generalized Birth-Death Stochastic Model for High Frequency Order Book Dynamics, *Quantitative Finance*, **12**(4), 547-557, 2011.

Karlin S. and McGregor J., Linear Growth, Birth and Death Processes, *Journal of Mathematics and Mechanics*, **7**(4), 1958.

Kendall D. G., On the Generalized Birth and Death Processes, *Ann. Math. Stat.*, **19**, 1-16, 1948.

Morgan B. J. T., Four Approaches to Solving Linear Birth and Death (and similar) Processes, *Int. J. Math. Educ. Sci. Technol.*, **10**(1), 51-64, 1979.

Novozhilov A. S., Karev G. P. and Koonin E. V., Biological Applications of the Theory of Birth and Death Processes, *Briefings in Bioinformatics*, **7**(1), 70-85, 2005.

Orsingher E. and Polito F., Fractional Pure Birth Processes, *Bernoulli*, 16(3), 858-881, 2010.

Trivedi K. S., Probability and Statistics with Reliability, Queuing and Computer Science Applications, 2nd edn., John Wiley and Sons Inc., UK, 2001.

Angular Power Spectrum

S. M. Mutunga, G. O. Okeng'o and C. O. Mito
Department of Physics, College of Biological and Physical Sciences, School of Physical Sciences, University of Nairobi, P.O Box 30197-00100 Nairobi, Kenya.
E-mails: gokengo@uonbi.ac.ke; collins@uonbi.ac.ke

Abstract
There is currently no general agreement amongst cosmologists as to whether the famous Copernican Principle (CP), a statement that we do not occupy any special location in the Universe, is valid or not. This has posed serious questions on our cosmological knowledge about the Universe. In this paper, we use data from the National Aeronautics and Space Administration (NASA), Legacy Archive for Microwave Background Data (LAMBDA) to assess the validity of the CP by studying the observed Cosmic Microwave Background (CMB) anisotropies, and the temperature angular power spectrum. Our results for the CMB temperature maps indicate the presence of anisotropies of the order 10^{-4} Kelvin, a magnitude lower than the theoretically predicted value of 10^{-5} Kelvin. By modeling the temperature angular power spectrum data and using the Wilkinson Microwave Anisotropy Probe (WMAP) seven-year and nine-year data, in comparison with Planck data, we deduce theoretical fitting formulae that may be used in constraining future cosmological models and in validating future CMB data.

1. Introduction

Establishing the validity of Copernican Principle (CP) – the assumption that we do not occupy any privileged location in the Universe, remains a key challenge in modern cosmology today, thus posing serious questions about the current standard cosmological model- called the "Lambda Cold Dark Matter" (LCDM) model (Clarkson *et al.*, 2008). In particular, its key prediction that our Universe is permeated by over 70% unknown and ubiquitous form of energy- called "dark energy", poses one of the greatest challenges in modern cosmology that requires resolution (Uzan, 2010).

Attempts to confront the challenges within the LCDM model have seen cosmologists shift their focus on one of its basic assumptions called the Copernican Principle (CP). The CP owes its origins in the proposal by Nicolaus Copernicus during the 16th century of a heliocentric Universe, and argues that we humans do not occupy any special location in the cosmos (Gingerich, 1993). The LCDM model, formulated within the framework of the Einstein's theory of general relativity relies on the CP assumption whose validity, however, has not been firmly established to date (Peebles, 1998).

In general, the CP assumes both homogeneity and isotropy of the Universe. Homogeneity suggests that the universe is composed of parts or elements that are of same kind, and as such one region of space is as good as another. Isotropy, on the other hand, infers that there is no preferred direction in space, that is, the Universe looks the same in all directions. Whereas current cosmological observations largely imply isotropy of the

Universe, homogeneity still remains unestablished to date (Maartens, 2011) with many studies focusing on high precision observations of the CMB using advanced satellite such as the Planck satellite.

The CMB radiation remains a great tool for helping test the CP and hence the LCDM model. Observation of this primordial radiation discovered accidentally in 1965 (Penzias and Wilson, 1965), believed to be the relic radiation from the big bang, yielded first CMB maps that provided evidence of tiny anisotropies in the very early Universe.

This paper presents results from a study that aims at testing the CP using CMB temperature anisotropies from currently available cosmological datasets. CMB temperature fluctuations data from WMAP survey is used to create CMB maps using the cosmological tool *Healpix,* and the temperature (TT) angular power spectrum derived, using the nine-year WMAP in comparison to Planck data. More importantly, the resulting TT angular power spectrum is modeled as an *Nth* power polynomial that accurately mimics the Planck data.

2. Theoretical Input

Measurements of the CMB radiation frequency spectrum, temperature and polarization states are completely stuffed with cosmological data with the most information being packaged in the temperature spectrum. The temperature power spectrum, $C\ell$, is a plot of the fluctuations per multipole moment ℓ, which is obtained by taking average measurements from every vantage point throughout the universe.

By definition, the spherical harmonics transform of the CMB temperature field $T(\hat{n})$, is expressible as (Bennett *et al.*, 1996)

$$T(\hat{n}) = \sum_{lm} a_{lm} Y_{lm}(\hat{n}) \quad . \tag{2.1}$$

Here; $\hat{n}$ is the direction on the sky, a_{lm} are the spherical harmonics coefficients and Y_{lm} are the spherical harmonics themselves.

Using equation (2.1), the CMB power spectrum can be defined as the expectation value of the square of the spherical harmonics coefficients and is expressible as

$$C\ell = <| a_{lm} |^2> = < a_{lm} a_{lm}^* > . \tag{2.2}$$

The power spectrum of the observed CMB fluctuations can therefore be plotted as

$$\ell(\ell+1)\frac{C\ell}{2\pi} . \tag{2.3}$$

The contribution over a range of values of ℓ can be given approximately by (Bennett *et al.*, 1996)

$$\int_{\ell}^{\infty} 2\ell' C_{\ell'} d\ell' = \int_{\ell}^{\infty} 2\ell'^2 C_{\ell'} \frac{d\ell'}{\ell'} , \tag{2.4}$$

for $\ell = 1$ and so $2\ell^2 C_\ell$ is proportional to the contribution of the fluctuations per unit $\ln \ell$, giving a flat geometry at large angular scales as well as bringing out a lot of structures at smaller scales.

This study demonstrates how the TT power spectrum of the CMB can be computed and modelled from raw data by the use of the publicly available WMAP data.

3. Research Methodology

3.1 Data acquisition

Acquisition of the WMAP seven year's temperature fluctuations data from the AstroML datasets was done using a python code that fetched the data and downloaded it from the archive to the local computer. Using the same procedure, we also downloaded both the seven years and nine years WMAP CMB temperature (TT) power spectrum data files from the LAMBDA website. We further acquired the Planck CMB temperature (TT) power spectrum data from the Planck website.

3.2 Creating and manipulating CMB maps

CMB maps provide a representation of an array of numbers for which each array element refers to a particular location in the sky. They produce a proper subdivision of a spherical surface so that each pixel covers the same surface area. Pixels are distributed on lines of constant latitude, which allows use of harmonic analysis applications involving spherical harmonics. The resolution of each map is controlled by a parameter that explains the quantity of divisions at the edge of a base resolution pixel that is expected to achieve the required high resolution allotment, called N_{Side}. Areas of all pixels at a given resolution are identical. For a given value of N_{Side} all pixel centers are located on a certain point that we call N_{ring} that can be defined by

$$N_{ring} = 4N_{side} - 1, \tag{3.1}$$

of constant latitude.

The total number of pixels in a given CMB map that we call N_{pix} can be determined as

$$N_{pix} = 12N_{side}^2. \tag{3.2}$$

Full sky CMB temperature fluctuations maps were created using a python code and with the help of Healpy, we were able to visualize the raw seven years WMAP CMB anisotropies data.

3.3 Masking

In order to achieve more qualitative analysis of the desired regions, a process of covering or hiding unwanted regions called masking was done. The CMB signal is contaminated by various types of foreground emissions that originate from both galactic and extragalactic sources leading to contamination in form of large temperature fluctuations

on the CMB maps. Masking was done to remove these contaminated regions of the sky. Their removal was made possible by taking the advantage of all the ways in which they differ from the CMB signal. Their frequency dependence was used to detect and subtract them. For example, in regions where these emissions were highly non-Gaussian, band pass filtering the map was done. In areas where the contaminations were localized in real space like the galactic, these emissions were down-weighted such that for low multipoles, high frequency channels were discarded while for high multipoles, low frequency channels were discarded.

3.4 Map Smoothing

To increase the signal quality with respect to the background, a process called smoothing was applied. The smoothing process aimed at boosting the Signal to Noise Ratio (SNR) which is a symbolic of the signal quality. The SNR is expressible as

$$SNR = \frac{P_{Signal}}{P_{noise}}. \tag{3.3}$$

where P is the average power. For this purpose, we performed a one degree smoothing on the masked CMB map.

3.5 Modelling the CMB temperature angular power spectrum

From the Legacy Archive for Microwave Background Data Analysis (LAMBDA) website, we acquired both the seven year and nine year WMAP temperature data of the CMB. After downloading these datasets, we realized a non-uniformity in the nine years data as compared to the seven years data. Certain multipole moment values in the nine years data did not have corresponding temperature values. To deal with this, we applied a simple extrapolation technique to fill in the gaps.

In order to model the TT angular power spectrum of the CMB, we used the gap filled data for the region $2 \le \ell \le 800$.

4. Results and Discussions

4.1 Results

Full sky CMB temperature map which we created using the seven-year temperature fluctuations data from AstroML datasets, is as shown in **Figure 1**;

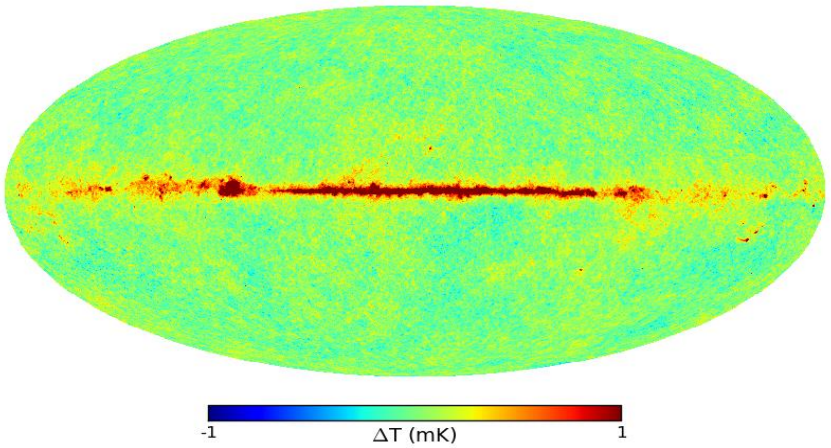

Figure 1: Full sky CMB temperature fluctuations map produced using raw seven years WMAP data.

Figure 1 displays almost uniform distribution of the temperature fluctuations of 1 miliKelvins (mK) with large deviations occurring along the galactic plane. However, if we assume the map to be divided in to northern part and southern part, along the galactic plane, then keen observation reveals a slight anomaly in the distribution of the temperature fluctuations. More deviations were noticeable in the southern section compared to the northern one. We demonstrated this by regulating the temperature deviations scale to run from $0.5\ mK$ to $1\ mK$ as shown in **figure 2**.

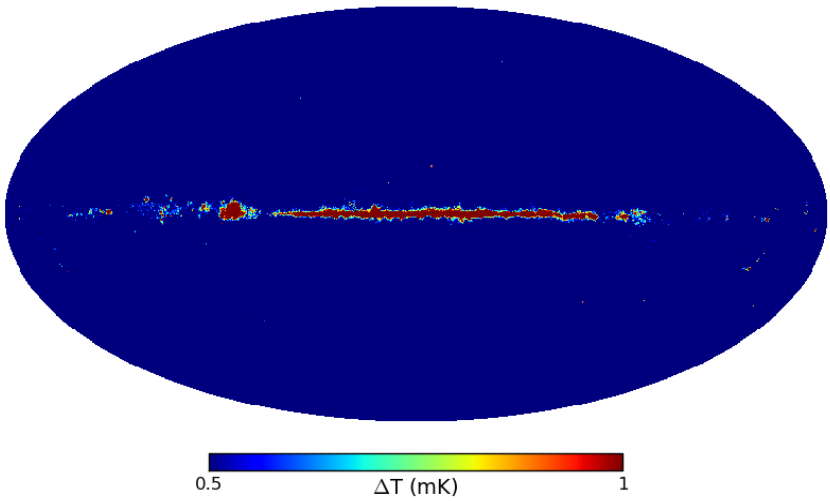

Figure 2: Full sky CMB temperature deviations map showing anomalies in their distribution. There are more deviations in the southern region compared to the northern one.

Application of masking on figure 1 yielded the CMB sky map shown in figure 3 below;

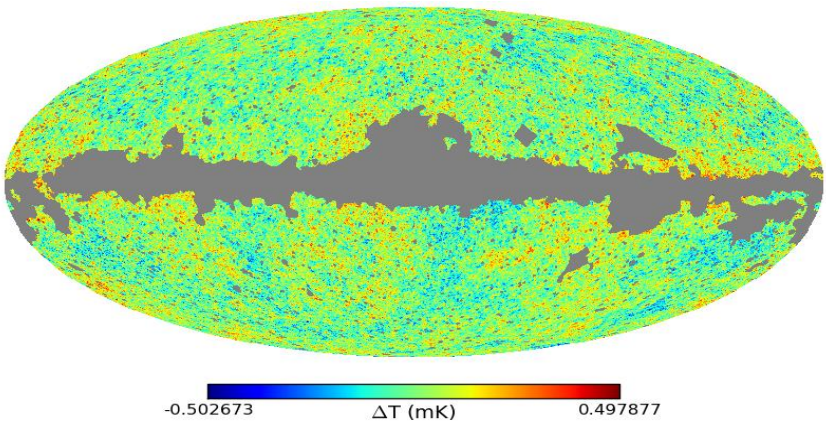

Figure 3: Masked full sky CMB temperature fluctuations map.

From Figure 3, it is notable that the temperature deviations reduced from the order of 10^{-3} to the order of 10^{-4}. We find these anisotropy levels not enough to violate the CP considering the fact that the homogeneity assumption is not confirmed. The conviction is that the universe was implicit base up design, implying that the little anisotropies observed in the CMB sky went about as gravitational seeds for the structure we see today. Over-dense areas pulled in more matter, while under-dense districts drew in less, and hence these little anisotropies in the CMB turned into the substantial scale structures we see in the universe today. This is in accordance to the standard model of cosmology. After carrying out a smoothing process on figure 3, we obtained **figure 4**; improved after smoothing.

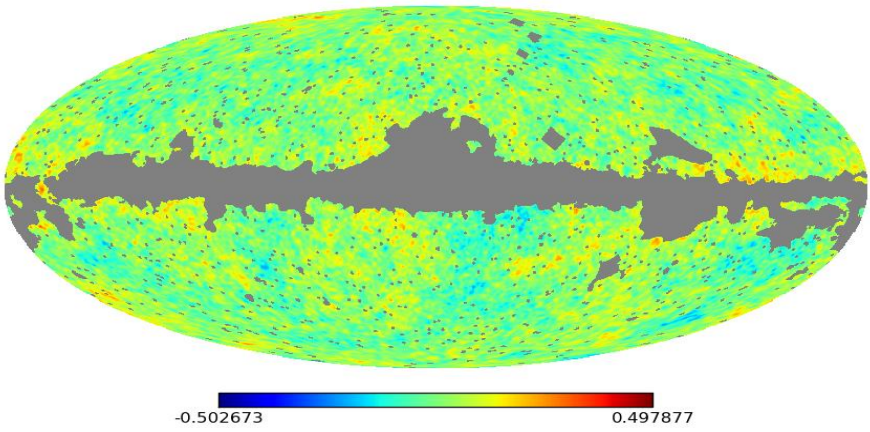

Figure 4: Masked full sky CMB temperature fluctuations map smoothed

Figure 4 has a good visual quality as compared to figure 3 since the signal quality was Results on the modelling of the CMB temperature angular power spectrum were as follows. We began by fitting the seven years TT angular power spectrum of the CMB with a polynomial and represented it in **figure 5**.

The data was found to be well fitted with an N^{th} order polynomial of the general form

$$F^n(\ell) = \sum_{i=0}^{n} A_i Z^n(\ell), \tag{4.1}$$

where $n = 0,1,2...N$, $i = 0,1,2,3...N$, A_i are the coefficients,

$Z(\ell) = \left(l - 4e + 002\right) \Big/ 2.3e + 002$ while l is the Multipole moment. In our case, $N = 8$.

Expanding equation (4.1) we obtained

$$F^{(n)}(\ell) = A_0 + A_1 Z(\ell) + A_2 Z^2(\ell) + A_3 Z^3(\ell) + A_4 Z^4(\ell) + A_5 Z^5(\ell) + A_6 Z^6(\ell) + A_7 Z^7(\ell) + A_8 Z^8(\ell) \tag{4.2}$$

.

The coefficients of equation (4.2) were obtained using MATLAB as to be

$$\begin{aligned}
A_0 &= 1.9e + 003 \\
A_{1=} &= -1.9e + 003 \\
A_2 &= 9.1e + 003 \\
A_3 &= -1.1e + 003 \\
A_4 &= -1.2e + 004 \\
A_5 &= 1.9e + 003 \\
A_6 &= 5e + 003 \\
A_7 &= -4.2e + 002 \\
A_8 &= -7.2e + 002
\end{aligned} \tag{4.3}$$

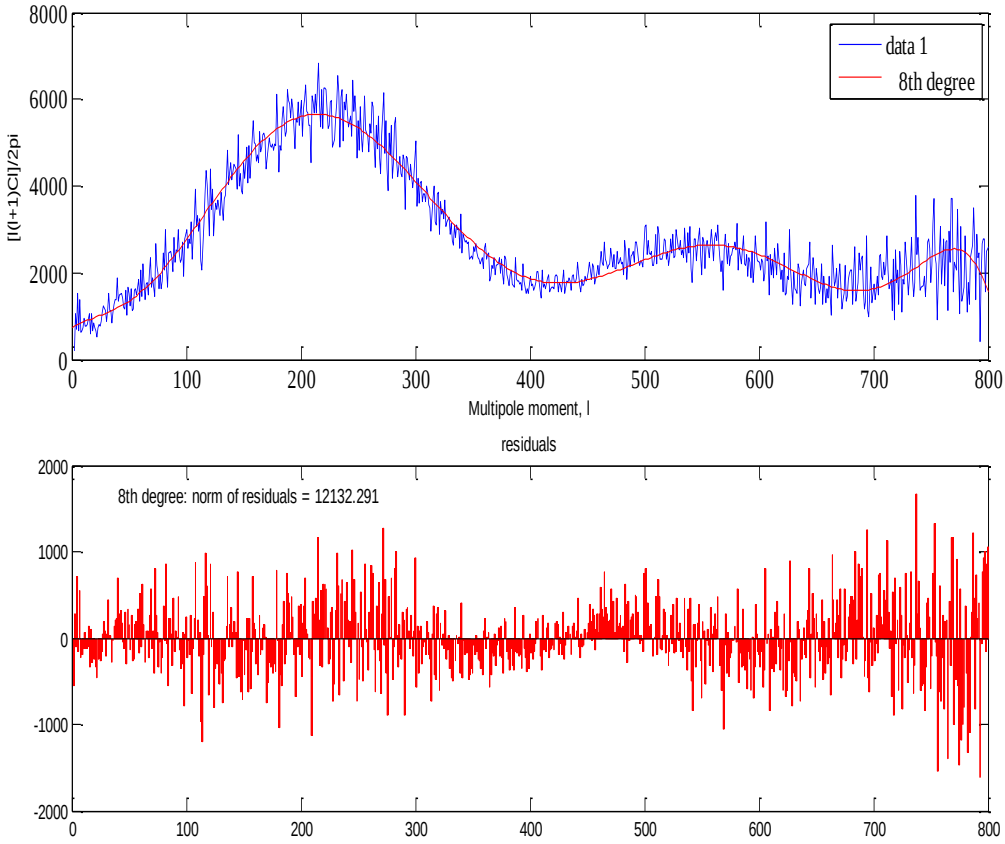

Figure 5: Seven years WMAP temperature data fitted with an 8th degree polynomial. The subplot is a graph of the residuals.

Similarly, we plotted a graph of the TT angular power spectrum of the CMB using the WMAP nine years data covering the same region, fitted the data with a polynomial and represented it in **figure 6**. We found out that the data could be well fitted with a polynomial equation of the same general form as equation (4.1) although the coefficients were different as shown

$$
\begin{aligned}
A_0 &= 1.9e+003 \\
A_1 &= -1.9e+003 \\
A_2 &= 8.9e+003 \\
A_3 &= -9.2e+002 \\
A_4 &= -1.1e+004 \\
A_5 &= 1.8e+003 \\
A_6 &= 4.8e+003 \\
A_7 &= -4e+002 \\
A_8 &= -6.9e+002
\end{aligned} \qquad (4.4)
$$

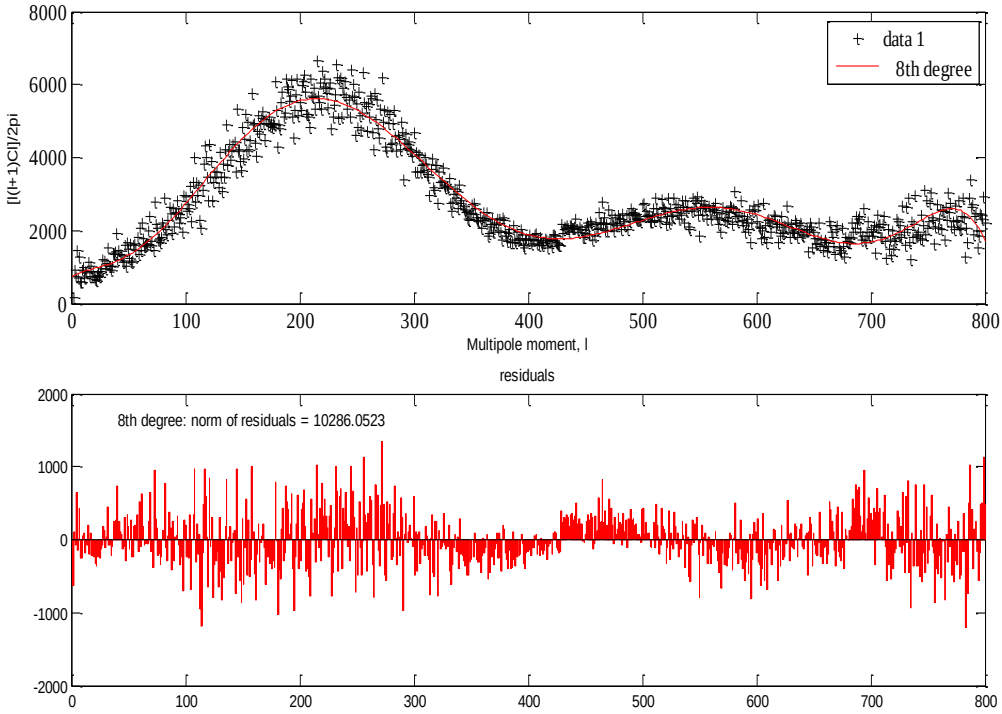

Figure 6: Nine years WMAP temperature data fitted with an 8th degree polynomial. The subplot is a graph of the residuals.

In order to obtain the best equation that can be used to model the TT angular power spectrum of the CMB, we plotted figure 1 and figure 2 together, that is, we superimposed both the seven years and nine years TT angular power spectrum of the CMB on the same axes for the region $l = 2$ to $l = 800$ and fitted the curve with a polynomial which we

present in **figure 7**;

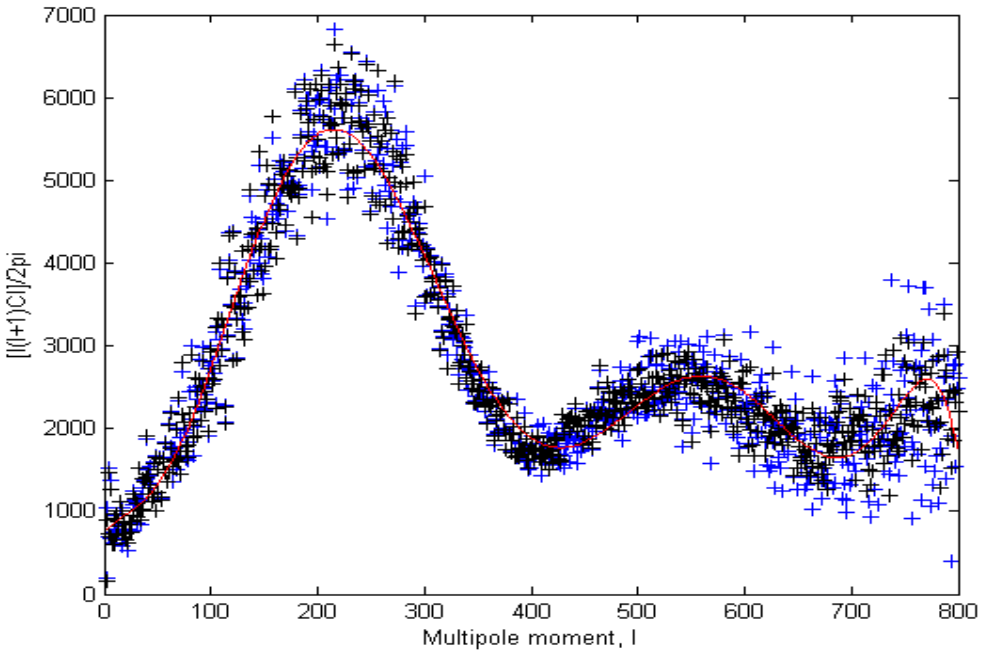

Figure 7: TT angular power spectrum of the CMB for both seven years and nine years WMAP datasets for $l = 2$ to $l = 800$, fitted with a polynomial. The blue data points are from seven years WMAP data while the black data points are from nine years WMAP data.

The equation for the polynomial that best fitted the two datasets was found to be of the same form as that of equation (5.1) and had similar coefficients as the ones represented in equation (5.4). An insight that the WMAP nine years data was more refined compared to the seven years data. This fit is the best model for the TT angular power spectrum of the CMB.

As a way of quantifying our results, we plotted a graph of the TT power spectrum of the CMB from seven years WMAP data against TT power spectrum of the CMB from nine years WMAP data. We then fitted a linear function on the plot to get the statistics on how the two datasets correlate with each other. We represent this in **figure 8** below

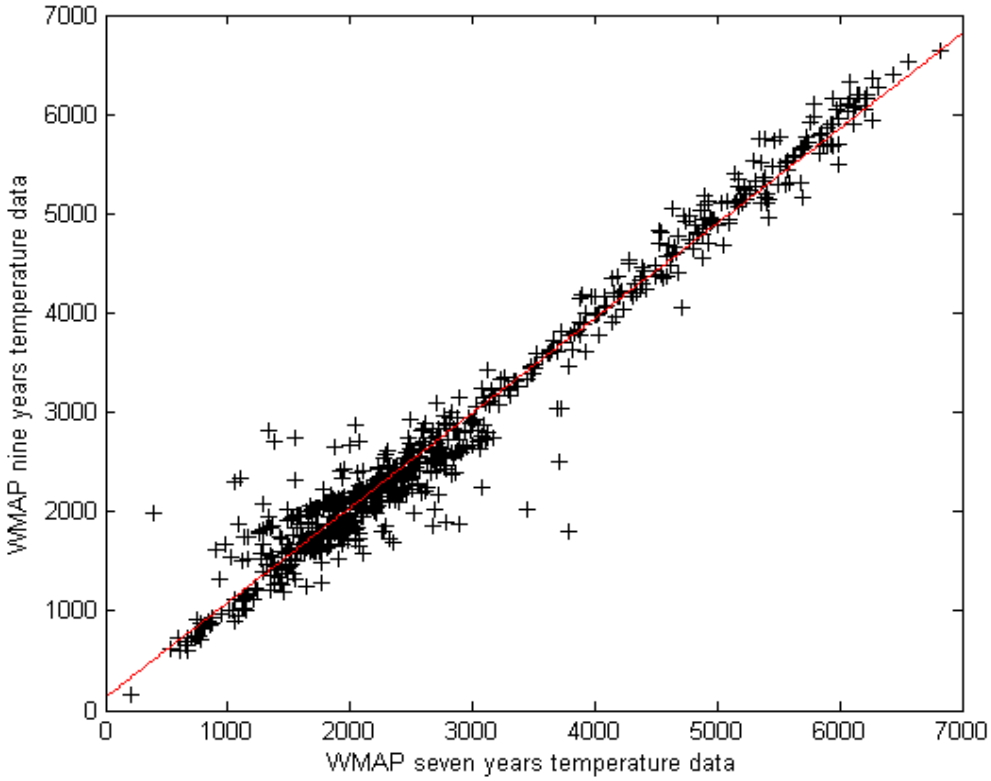

Figure 8: Nine years temperature data against seven years temperature data for $2 \le l \le 800$.

We obtained the equation relating the nine years TT (TT_9) data to seven years TT (TT_7) data for $2 \le \ell \le 800$ to be

$$TT_9 = 0.95TT_7 + 130. \tag{4.5}$$

Equation (4.5) is a model equation that showed a strong positive correlation between the two datasets. From equation (4.5), it is notable that when $TT_7 = 0,\ TT_9 = 130$.To carry out sensitivity analysis of this model, we neglect the y-intercept of equation (4.5) so that we have

$$TT_9 = 0.95TT_7. \tag{4.5a}$$

From equation (4.5) we find that, when $TT_7 = 1,\ TT_9 = 0.95$. This implies that, 1% change in TT_7 would cause 0.95% change in TT_9.

As a way of validating our temperature angular power spectrum model, we used Planck temperature data which is a high resolution data compared to WMAP data.

We superimposed our obtained model with Planck data and as shown in **figure 9**;

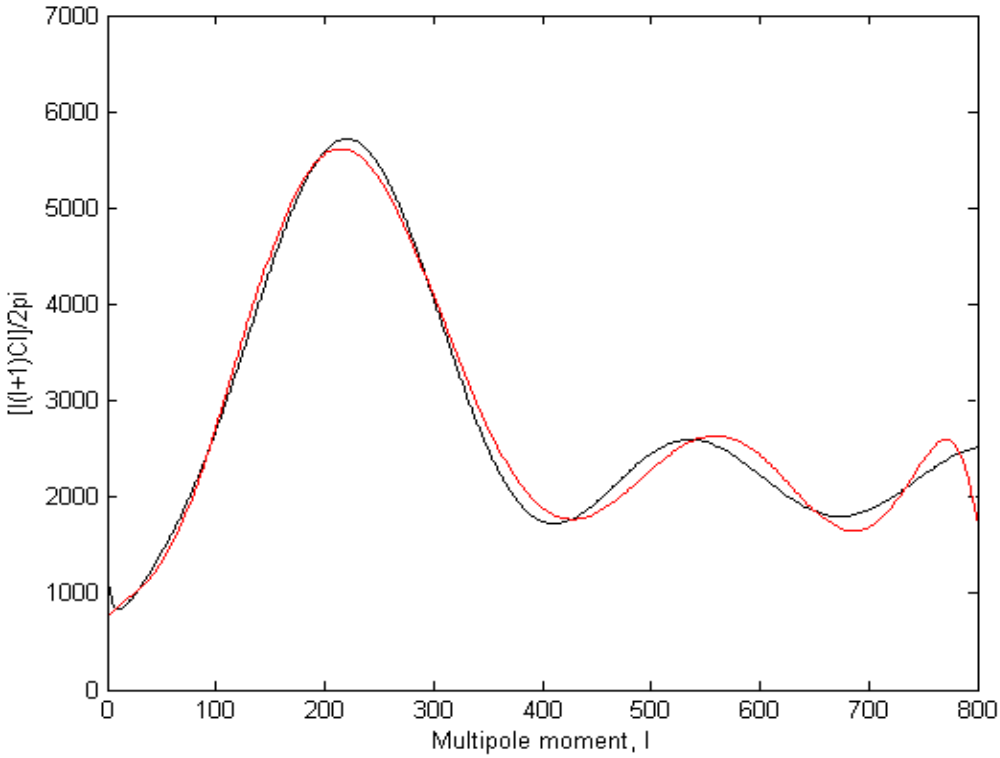

Figure 9: TT angular power spectrum model compared with the TT angular power spectrum from Planck data. The black curve represents the Planck data while the red curve is the model.

Since our model was found to be the best fit for the WMAP nine years TT power spectrum data, we sought out the relationship between the Planck temperature data and the WMAP nine years temperature data. This was done by plotting a graph of the Planck temperature data against the WMAP nine-year temperature data. We did a linear fit to the data in order to get an equation relating the two datasets. This comparison was done for values of multipole moments, $l = 2$ to $l = 800$ and is represented in **figure 10**;

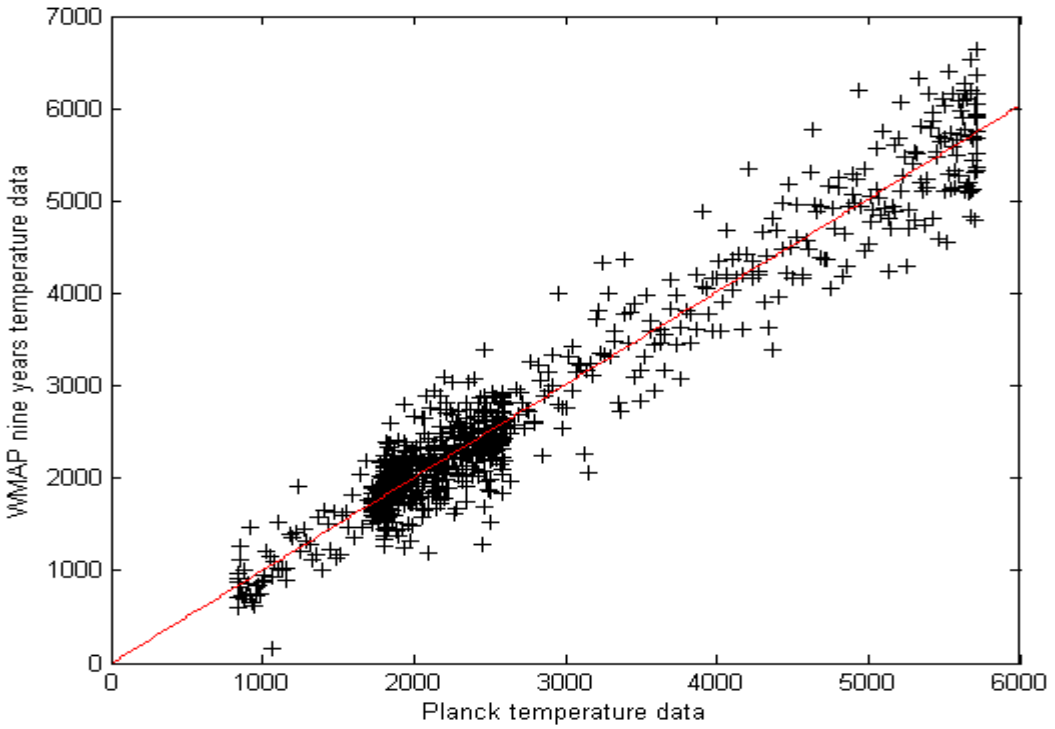

Figure 10: WMAP nine years' temperature data against Planck temperature data**.**

We obtained the equation relating the two datasets, the Planck TT (TT_P) data and the WMAP nine years TT (TT_{W9}) data to be

$$TT_{W9} = TT_P - 5.1. \tag{4.6}$$

Equation (4.6) showed a strong positive correlation between the two datasets with only a slight lag. The linear correlation coefficient r, between the two datasets was found to be *0.975*. Further the coefficient of determination r^2, was obtained to be *0.951*. It is the goodness of fit explaining how Planck data is replicated by the model. 95.1% variations of Planck data are explained by the model, the remaining 4.9% are either explained by the variable(s), not included in the model or are absorbed by the error term of the model.
This strong correlation was a justification of our TT model to be valid since it was the best fit for the WMAP nine-year temperature data.

5. Discussions

From our results of the CMB maps, we found slight temperature deviations that corresponded to areas of different densities at very early times. The observed temperature deviations in the CMB were found to be of sizes of the order of $10^{-3}\ K$. However, these fluctuations reduced after performing masking and smoothing processes to sizes of the order of $10^{-4}\ K$. We found these anisotropy levels not enough to invalidate the CP.

This outcome is in respect to the standard model of cosmology which explains that the fluctuations arose immediately after the Big Bang and were stretched to cosmologically large scales during a brief period of accelerated expansion known as inflation. In the chance that the universe is smooth but not consummately smooth, then gravity will make structure to develop, by drawing matter into districts that begin over the average densities and out of regions that begin underneath the average density. Tentatively, for this procedure to work, there probably had been little adequacy inhomogeneities present in the early universe, which served as the "seeds" for the gravitational development of structure. These inhomogeneities ought to bring about slight non-consistencies in the CMB. Since the standard cosmological model is founded on the basis of the CP, this result at the moment upholds the CP. However, high precision measurements of the CMB anisotropy can help to delineate this enigma for example by shedding more light on the anomaly noted in the distribution of the fluctuations. Furthermore, studies to proof the homogeneity of the universe will greatly influence the confirmation of the CP.

Conversely, the equation (4.5) derived in this study is very useful as it can be used to reproduce either of the datasets if some points are missing. The TT angular power spectrum model obtained in this work could be useful in constraining future cosmological models since it is computed from data. The model shows good validity, as it agrees well with high resolution data from Planck. The theoretical model being the best fit to the WMAP nine years' temperature data with a coefficient of determination (r^2) of ***0.951*** in relation to the Planck data, further supports its validity.

6. Conclusions

This study aimed at assessing the validity of the CP using observed anisotropies in the CMB and modeling the TT angular power spectrum. We used WMAP seven years temperature fluctuations data contained in the AstroML datasets to create CMB maps. It was found that the CMB signal is dominated with various foreground emissions which are both galactic and extragalactic. These contaminations caused temperature deviations of the order of $10^{-3}K$. When a clean-up process called masking was done, these areas were excluded making the temperature fluctuations of the CMB map to drop to the order of $10^{-4}K$. A smoothing process was done to improve the signal strength. The tiny temperature fluctuations of the CMB map can be associated with the slight inhomogeneities in the matter density in the early universe that seeded the current structure. The disclosure of these little deviations from smoothness (anisotropies) in the CMB is welcome for it gives in any event the likelihood to the seeds around which structure formed in the later universe.

In this light, we can conclude that, we owe our extremely existence to this evident fluctuations for without the density fluctuations that they flag, there would have been no galaxies, no stars, no solar system and no humans. This outcome is in respect to the standard model of cosmology which explains a smooth universe characterized by some perturbations. It is a justification to the Copernican Principle (CP) since the standard model has its foundations on it.

Moreover, using the acquired seven years and nine years WMAP TT data from the LAMBDA website, we modelled the TT angular power spectrum of the CMB. Equation (4.5) which relates both the WMAP seven years and nine years TT data was also obtained. It is useful for it can be used to reproduce either of the datasets if some points are missing. The obtained model was found to agree well with Planck TT data and it is useful for it can be used to produce the TT angular power spectrum in the absence of data and to constrain future cosmological models since it is computed from data.

Acknowledgements
We would like to thank the administration of the university of Nairobi for sponsoring this work and the Legacy Archive for Microwave Background Data Analysis (LAMBDA), part of the High Energy Astrophysics Science Archive Center (HEASARC) which is a service of the Astrophysics Science Division at the NASA Goddard Space Flight Center for the provision of the data used in this work. We also acknowledge Professor G. Pokhariyal for his expertly advise.

References

Bennett, C. L., Banday, A., Gorski, K. M., Hinshaw, G., Jackson, P., Keegstra, P., Kogut, A., Smoot, G. F., Wilkinson, D. T., and Wright, E. L. (1996). 4-year COBE DMR cosmic microwave background observations: maps and basic results. *ArXiv Prepr. Astro-Ph9601067*.

Clarkson, C., Bassett, B., and Lu, T. H.-C. (2008). A general test of the Copernican Principle. *Phys. Rev. Lett.* **101**, 011301.

Gingerich, O. (1993). The eye of the heaven. Ptolemy, Copernicus, Kepler. *In* "Masters of modern physics," Vol. 7.

Maartens, R. (2011). Is the Universe homogeneous? *Philos. Trans. R. Soc. Lond. Math. Phys. Eng. Sci.* **369**, 5115–5137.

Peebles, P. J. E. (1998). The standard cosmological model. *ArXiv Prepr. Astro-Ph9806201*.

Uzan, J.-P. (2010). Dark energy, gravitation and the Copernican principle. *Dark Energy Obs. Theor. Approaches*.

Guide to contributors

Papers submitted for publication should be sent to the Editor, Kenya National Academic of Science, and P.O. Box 4618-00100, Nairobi - Kenya. They should be of original research in the field of science and technology. Authors should submit a softcopy containing the original manuscript, done preferably in Word or similar word processing software. No manuscript should be submitted in the pdf format.

Papers must not have been published or accepted for publication elsewhere. They will not necessarily be published in order of the receipt; those that require little editing are likely to appear earlier than those that involve much. For general guidance on matters of presentation and style contributors are advised to consult the *General Notes on the Preparation of Scientific Papers, London: Royal Society*,1965, and *Guide for the preparation of Scientific Papers of Publications,* Paris; UNESCO, 1968.

Text should be typewritten (double-space, with ample margin and one side of the paper only). Titles should be as brief as in consistence with clarity. Abbreviations should conform to *British Standard* 1991, Part 1, 1967. Metric Units are preferred; if non-metric units are used metric equivalents should be given at least once in each paper. Footnotes should be avoided. The form of article preferred provides seven major divisions summary brief introduction, methods, results, discussion, conclusions, acknowledgement and references. Italics should be marked in manuscripts by single underlining. Scientific names of general species and varieties must be in italics, but the authority in roman type e.g., *Spodeoptera exempta* walk. Scientific names of high groups (orders, classes and families) are printed in roman type, e.g., Caniferae,

Tables should be reduced to the simplest form and, numbered in Arabic numerals.

Line drawings and graphs must be in jet-black Indian ink on Bristol board or tracing cloth (using pens and stencils of even thickness and density) and must be completed (inclusive of all letters and numerals in the figures themselves) by the author in a form suitable for reproduction. They must be drawn to a scale that will permit their reduction (preferably by one-third) to an area not exceeding 18 x 12 cm inclusive of legend. Figures should be numbered in Arabic numerals and their desired position in the text. The Author`s name and title of the paper must be written on the back of each illustration.

Photographs for reproduction as plates are admissible (two plates per paper are permitted and additional plates must be paid for by the authors or his department). Authors should supply unmounted glossy prints, with good contrast, numbered and marked lightly on the back with author's name, title of paper and a clear indication of the top and bottom of the picture. (It would be appreciated if authors would mention of illustrations, figures, etc., enclosed.)

Papers must include a short factual summary, complete in itself, giving results obtaining and conclusion reached, not exceeding 3% of the length of the paper before the introduction.

Reprints:
First authors receive 15 copies of their papers free of charge, and they may buy additional copies if ordered before publication.

Short Communications:
A special section under the above title will be included in the journal as necessary to cater for short articles which do not qualify for publication as scientific papers.

These are short articles, normally of not more than 500 words which report:-

1. Research results which are complete but do not warrant comprehensive treatments, e.g., descriptions of new cultivars improved technique and equipment with supporting data.
2. Research work which is incomplete and not likely to be concluded to the point where it would be reported in a conventional scientific paper.
3. Other useful research findings and developments which in the opinion of the editor would be of value if published promptly.

Table of Contents

Sensitivity Analysis of Cisco 12000 GSR

Musiga L. A..... 1-9

Geometric and Physical Properties of Curvature Tensors

Pokhariyal G.P., ... 10-18

Non-Birth-Death Continuous Time Markov Chain Availability Models with Exponentially and Non-Exponentially Distributed Unplanned Outages

Musiga L. A., Ottieno J. A. M., and Weke P.G. O……..19-35

On Testing the Copernican Principle: Modeling the CMB Temperature Angular Power Spectrum

S. M. Mutunga, G. O. Okeng'o and C. O. Mito 36-50

© The Kenya National Academy of Sciences

0250-8265 ISSN CODEN KSTSDG